REPORT DOCUMENTATION PAGE

Form Approved OMB No. 0704-0188

1. REPORT DATE *(DD-MM-YYYY)*	2. REPORT TYPE	3. DATES COVERED *(From – To)*
06-05-2008	Final Report	1 March 2005 - 22-Jul-10

4. TITLE AND SUBTITLE

ADVANCED SINGLET OXYGEN GENERATOR FOR A COIL

5a. CONTRACT NUMBER
FA8655-05-C-4022

5b. GRANT NUMBER

5c. PROGRAM ELEMENT NUMBER

6. AUTHOR(S)

Dr. Jarmila Kodymová

5d. PROJECT NUMBER

5d. TASK NUMBER

5e. WORK UNIT NUMBER

7. PERFORMING ORGANIZATION NAME(S) AND ADDRESS(ES)
Institute of Physics Academy of Science
Na Slovance 2
182 21 Prague 8
Czech Republic

8. PERFORMING ORGANIZATION REPORT NUMBER

N/A

9. SPONSORING/MONITORING AGENCY NAME(S) AND ADDRESS(ES)

EOARD
Unit 4515 BOX 14
APO AE 09421

10. SPONSOR/MONITOR'S ACRONYM(S)

11. SPONSOR/MONITOR'S REPORT NUMBER(S)
SPC 05-4022

12. DISTRIBUTION/AVAILABILITY STATEMENT

Approved for public release; distribution is unlimited.

13. SUPPLEMENTARY NOTES

14. ABSTRACT

This report results from a contract tasking Institute of Physics Academy of Science as follows: The first year (2005)
· A conceptualization of the problem including a theoretical estimation of SOG parameters (based on preliminary results of the current grant awarded for 2004) particular problems, calculations, design of generator concept;
· A technical design of individual parts of SOG (elaboration of technical drawings);
·A review and purchase of suitable BHP spray nozzles and necessary diagnostics units
·Manufacturing of some device parts.
The second year (2006)
·Testing of individual parts of SOG with a model liquid (some BHP like solution), study of aerosol properties by suitable diagnostics (e.g. Beam scattered-light sensor);· Modification of SOG design based on experimental results with the model liquid;
·Completion of the SOG device and starting with the device testing using BHP solution
The third year (2007)
·Investigation of output SOG parameters (i.e., O2(Dg) yield, water vapor content, chlorine utilization)
Testing the SOG coupled to a 5-cm-gain COIL nozzle plenum

15. SUBJECT TERMS
EOARD, Laser physics, Lasers, Laser engineering

16. SECURITY CLASSIFICATION OF:			17. LIMITATION OF ABSTRACT	18, NUMBER OF PAGES	19a. NAME OF RESPONSIBLE PERSON
a. REPORT	b. ABSTRACT	c. THIS PAGE			A. GAVRIELIDES
UNCLAS	UNCLAS	UNCLAS	UL	37	19b. TELEPHONE NUMBER *(Include area code)* +44 (0)1895 616205

DEPARTMENT OF THE AIR FORCE

HEADQUARTES, 603D REGIONAL SUPPORT GROUP (USAFE)

European Office of Aerospace Research and Development (EOARD)

Final Report of the Contract

Referring to

Contract No. 054022, Award No. FA8655-05-C-4022

Effective date 1 March 2005

Title: **Advanced singlet oxygen generator for a COIL**

Investigators: Otomar Špalek, Vít Jirásek, Miroslav Censký,
Jarmila Kodymová, Irena Picková, Jan Hrubý
Department of Chemical Lasers
Institute of Physics AS CR

Prime supervisors: Dr. Timothy Madden
Dr. Kevin Hewett
USAF Research Laboratory /DED, Kirtland AFB, NM

Contractor: Institute of Physics of Academy of Sciences CR
Dr. Jarmila Kodymová
Na Slovance 2
182 21 Prague 8
Czech Republic

Phone: +420 266 052 699
Fax: +420 286 890 265
E-mail: kodym@fzu.cz

Date of submission: 30 April 2008, 36 months after the Contract award

Contents

1. General outline of the Contract

1.1. Outline of the Contract subject and goals

Development of advanced generators of singlet oxygen (SOG) is one of challenges for a high-power chemical oxygen-iodine laser (COIL). Chemical generators of the jet-type and rotating disc-type employed hitherto in the conventional COIL systems can provide fairly high concentration of singlet oxygen; their operation parameters have however certain limitations for high-power lasers.

This three-year EOARD contract has been awarded for development of a new concept of advanced SOG device, construction of a small-scale SOG prototype, and investigation of the device operation. The following requirements for the novel SOG device were defined by the US AFRL/DED:

- A high-pressure operation, exceeding 100 Torr (~13 kPa) of oxygen pressure and containing an adequately high $O_2(^1\Delta)$ partial pressure;
- A single BHP pass burn down operation (no BHP circulation system employed); possibly to use a dilute BHP to maintain a thermal control and so to limit H_2O vapor;
- A close coupling of the generator to the laser nozzle plenum for minimizing $O_2(^1\Delta)$ transport loss;
- An efficient disengagement of gas/liquid (conceptually involving the angular acceleration of fluid and gas or both)
- A scalability to be suitable for the airborne and mobile applications

1.2. Tasks and supplies in the Contract proposal

Research phase 1 (1 March 2005 – 28 February 2006)

- Conceptualization of the problem based on theoretical estimation of the SOG parameters by computational modeling and calculations; elaboration of the new generator concept called a Centrifugal Spray Singlet Oxygen Generator (CentSpraySOG);
- Technical design of individual parts of the CentSpraySOG including elaboration of technical drawings;
- Survey and purchasing nozzles suitable for a BHP spray formation; to gather needed diagnostic techniques for investigation of the spray properties (e.g. the Beam Diffraction light Sensor for droplet size measurements), and parameters of generator exiting gas and liquid ($O_2(^1\Delta)$ yield, Cl_2 and BHP utilization);
- Fabrication and construction of the spray SOG device with a stationary performance (a spray reactor without a centrifugal gas-liquid separation) and investigation of the spray characteristics with a model BHP-like liquid;

Research phase 2 (1st March 2006 – 28th February 2007)

- Experimental investigation of the SOG parameters (i.e. $O_2(^1\Delta)$ yield, Cl_2, and BHP utilization) on the stationary spray device;

- Fabrication of mechanical parts of centrifugal separator, its assembling with a computer controlling system, and data acquisition system;
- Completing the CentSpraySOG device, starting with testing;

Research phase 3 (1st March 2007 – 28th February 2008)

- Systematic study of the CentSpraySOG parameters, i.e. the $O_2(^1\Delta)$ yield, Cl_2, and BHP utilization, and efficiency of the gas-liquid separation by the centrifugal separator;
- Testing the CentSpraySOG device coupled to a 5-cm-gain COIL nozzle plenum;

2. Summary of principle and theoretical estimations of CentSpraySOG operation

2.1. Principle

This generator takes advantage of the spray (also mist or aerosol) gas-liquid technology. A much larger interface area between the Cl_2 gas and BHP (basic hydrogen peroxide) liquid is produced, and so a short diffusion path of HO_2^- ions from bulk BHP liquid results in more efficient $O_2(^1\Delta)$ production than in other types of chemical generators (a jet-type or disk-type SOG). This makes possible to attain a very high reaction rate per unit reactor volume. Exhausted BHP liquid (droplets) is separated from the gas phase by impact and the centrifugal force in centrifugal separator that forms an inherent part of the whole compact SOG device. Simplified schemes of the generator and two-phase spray nozzle are shown in **Figs. 1a** and **1b**.

A fine spray is formed using a suitable nozzle from BHP and Cl_2/He mixture.

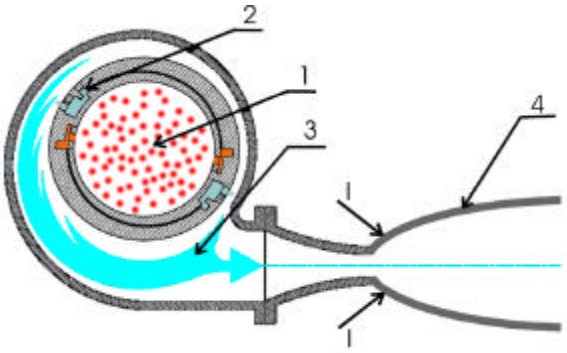

Fig. 1a. Scheme of CentSpraySOG coupled to laser nozzle. 1-spray of BHP-Cl_2/He mixture, 2-rotating separator, 3- gas stream with $O_2(^1\Delta_g)$, 4-laser nozzle, I-iodine injection

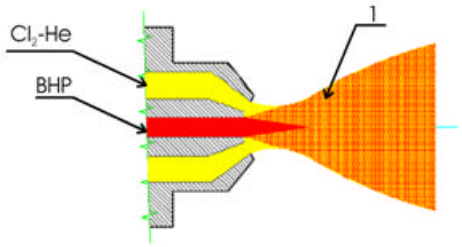

Fig. 1b. Scheme of two-phase spray nozzle. 1-spray of BHP-Cl_2/He mixture

The nozzle generating such a fine BHP spray is a crucial component of the generator and should meet by modeling results several important criteria: *(i)* to provide the optimal droplet size of ~20 μm; *(ii)* to generate droplets of uniform diameter to better optimize the Cl_2 utilization, U_{Cl}, BHP utilization, U_{BHP}, and $O_2(^1\Delta)$ yield, Y_Δ.; *(iii)* a two-phase nozzle has to be used for atomization of very viscose BHP liquid (5–35 mPas) by a pressurized gas; nozzles with external mixing of gas and liquid flows are preferred to control both flows independently; (iv) the spray with full cone shape is suitable for a cylindrical reaction space of the CentSpraySOG.

A cross-section (perpendicular to the axis of rotation) of the rotor of the centrifugal separator and its 3-D view are shown in **Figs. 2a** and **2b.**

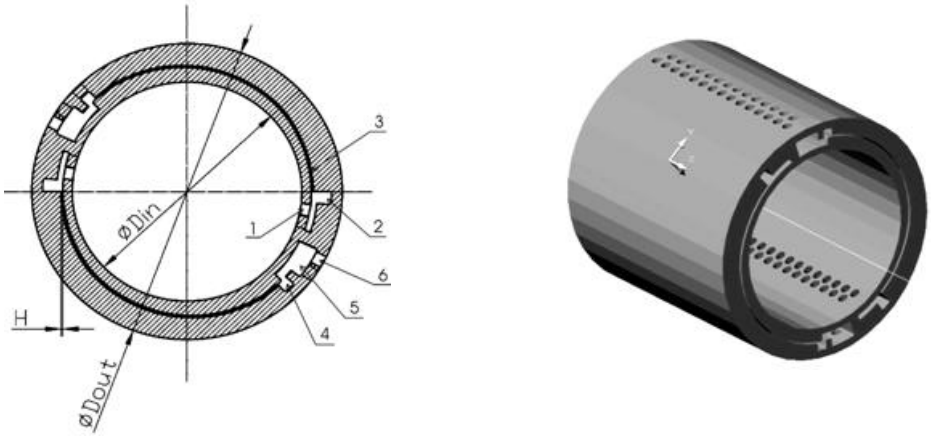

a) **b)**

Fig. 2. Cross-section and 3-D view of the centrifugal separator reactor diameter D_{in}= 37 mm, separator outer diameter D_{out} = 50 mm, reactor length a = 50 mm, 29 impactor holes of diameter d_i = 3 mm (in each channel), slit height H = 0.8 mm, slit length L_{slit}= 43 mm.

A central cylindrical part creates the reaction space for $O_2(^1?)$ generation from the BHP spray. A two-step separation of liquid from the gas flow containing $O_2(^1\Delta)$ runs as follows: (i) larger droplets of the spray impact on the inner walls of rotating „drum“ and in the impactor holes 1 of the rotor; the liquid is drained through channels 2; (ii) finer droplets remaining in the gas are removed in two narrow annular channels 3 by the centrifugal force and drained through channels 4. The gas with $O_2(^1?)$ leaves the separator through channels 5 and holes 6. Principle of the impact separation is illustrated for one impaction hole in **Fig. 3,** and a typical characteristic of the impactor in **Fig. 4**.

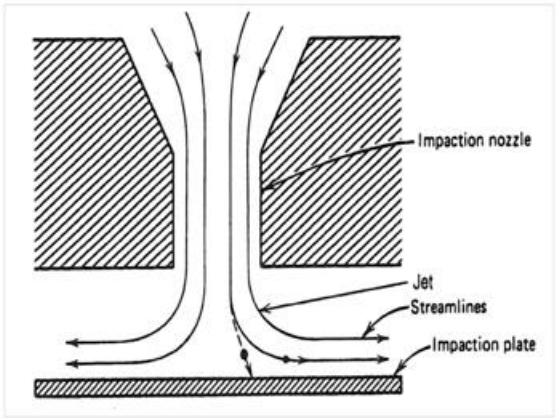

Fig. 3. Principle of the impactor separator [6]

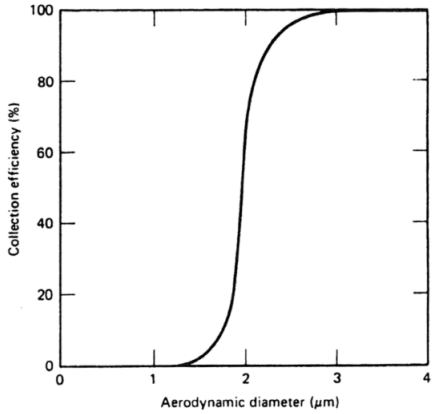

Fig. 4. Typical collection efficiency of impactor [6]

Theory and experimental facts on impactors have been well elaborated in the aerosol technology for collecting aerosol particles from air [6]. The aerosol-containing gas is accelerated in the impaction hole and impacts on the wall owing to bending streamlines at small radius of curvature. By inertia, droplets follow rather straight trajectories and impact on the wall. A collection efficiency of impactor, i.e. the fraction of captured particles (droplets) depends strongly on a droplet diameter. Characteristic droplet diameter corresponds to 50%-collection efficiency.

2.1. Theoretical estimations

2.1.1. Modeling of the spray reactor

A detailed theoretical model was developed and solved by computational modeling, based on general relations for description of the transport phenomena in gas-liquid reaction systems [1,2], theoretical analysis of oxygen-iodine laser [3], and previous theoretical and experimental investigations on the aerosol medium applied for the $O_2(^1\Delta)$ generation [4,5]. Model calculations were performed for the BHP spray with droplets of 20 μm and 10 μm, respectively. By preliminary results, the $O_2(^1\Delta)$ partial pressure could attain 5.5 kPa (40 Torr) and 15 kPa (110 Torr) within extremely short time of 6 ms and 1.4 ms, respectively [7]. Further model calculations were performed for the BHP spray produced by a selected nozzle (SAM-05-03, BETE Fog Nozzle, Inc., MA, USA) [8]. The input data for these calculations are summarized in **Table 1**.

Tab. 1
Input data for the spray SOG model calculations

Gas input	Cl_2/He mixture 1 : 4
Total gas flow rate	n_{tot} = 115 mmol s^{-1}
Total generator pressure	37.5 kPa (281 Torr)
Diffusion coefficient of Cl_2 in gas	D_{Cl} = 1.04 x 10^{-4} m^2 s^{-1}
Spray temperature	T = 260 K
BHP droplet diameter	d = 20 μm
Initial HO_2^- concentration in BHP	c_{H02-} = 5 or 8 M (kmol m^{-3})
BHP flow rate	V_L = 15 cm^3 s^{-1}
Diffusion coefficient of Cl_2, HO_2^-, O_2 in liquid	D = 5 x 10^{-10} m^2 s^{-1}
Sticking probability of Cl_2 on BHP surface	γ_{Cl} = 0.0075
Sticking probability of $O_2(^1\Delta_g)$ on BHP surface	γ_Δ = 0.003
Henry constant of chlorine	H_{Cl2} = 1
Henry constant of oxygen	H_{O2} = 20
Rate constant of reaction (3)	K_3 = 5 x 10^8 m^3 $kmol^{-1}$ s^{-1}
Lifetime of $O_2(^1\Delta_g)$ in liquid	$t_?$ = 2 x 10^{-6} s
Rate constant of $O_2(^1\Delta_g)$ quenching in gas	$*k_?$ = 3.7 x 10^4 m^3 $kmol^{-1}$ s^{-1}

3.

$^*k_?$=3.7x10^4 $m^3$$kmol^{-1}$$s^{-1}$ (i.e., 6.1x10^{-17} $cm^3$$s^{-1}$) is the sum of rate constants for reactions (10) and (11) in chap. 3.3.23.

The model evaluates a time course of the surface HO_2^- concentration, the mean HO_2^- concentration in droplet, the surface and bulk concentrations of chlorine and $O_2(^1\Delta_g)$. Then a maximum $O_2(^1\Delta_g)$ partial pressure and a time of attaining it was evaluated. **Figs. 5** and **6** show dependences of the BHP utilization, U_{BHP}, Cl_2 utilization, U_{Cl2}, $O_2(^1\Delta)$ yield, Y_Δ, and the "optimal" reaction volume, V_r, on a total pressure in the generator. The volume V_r followed from the product of total volumetric BHP spray

flow rate and time of achieving the maximum $O_2(^1\Delta_g)$ partial pressure. A heat release in the reaction system was not taken into account in this simplified model.

Main conclusions of these theoretical estimations are: (i) U_{BHP} values are fairly high (by two orders higher nearly than in a jet SOG); (ii) U_{Cl2} is above 0.9 with 8 M-BHP and ~0.8 with 5 M-BHP; (iii) Y_Δ is between 0.8-0.7 (higher values are with a more concentrated BHP due to a lower reaction depth for the $O_2(^1\Delta_g)$ production); (iv) the maximum V_r was 55 cm^3 and decreased fast with increasing generator pressure.

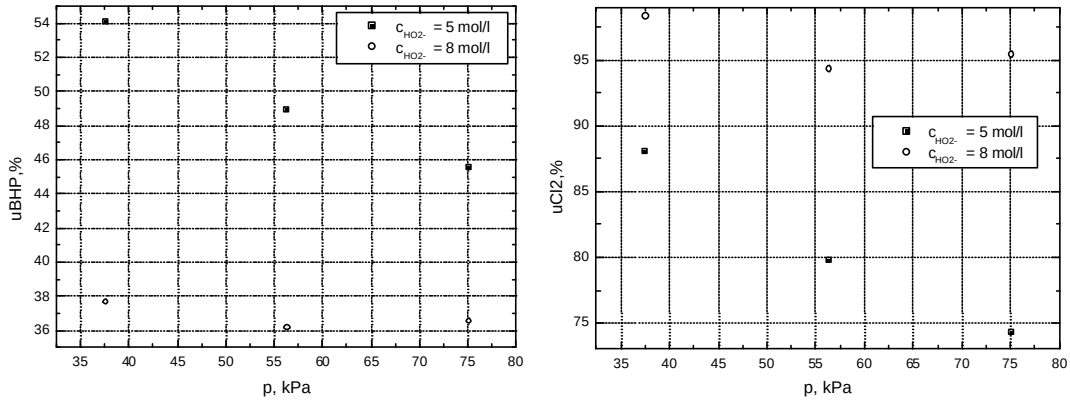

a) **b)**

Fig. 5. BHP utilization (a), and Cl_2 utilization (b) in dependence on total generator pressure. Nozzle SAM-05-03, d = 20 μm, v_{BHP} = 15 ml/s, n_{Cl2} = 23 mmol/s, n_{He} = 92 mmol/s

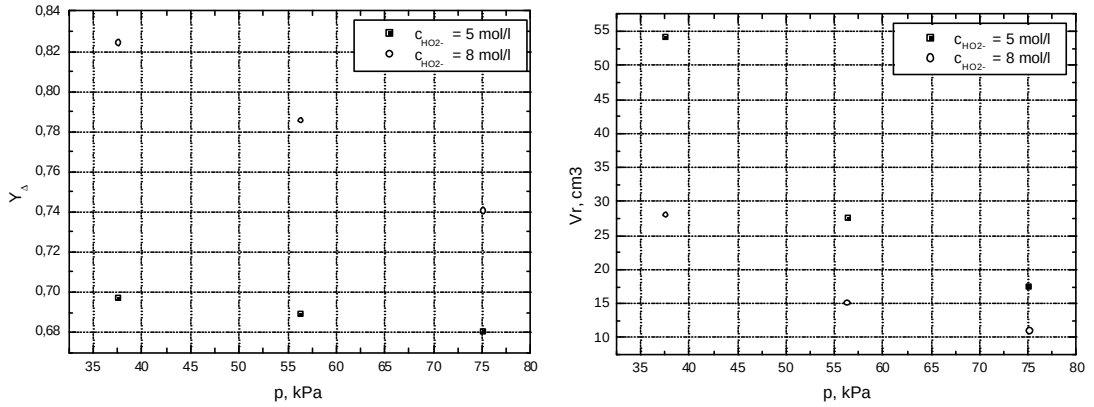

a) **b)**

Fig. 6. Singlet oxygen yield (a), and optimal reactor volume (b) in dependence on total generator pressure. Conditions the same as in caption of Fig.5

In further calculations were included the enthalpies of Cl_2/BHP reaction, dimolar $O_2(^1\Delta)$ quenching reactions and water evaporation. The results of final spray temperature and relative water vapor pressure, p_w/p_{O2}, are given in **Table 2.**

Tab. 2
Calculated U_{Cl2}, Y_{Δ}, final spray T, and ratio of water pressure to oxygen pressure, p_w/p_{O2}, for two values of generator pressure and BHP concentration, and nozzle SAM 05-03;
n_{gas} = 115 mmol/s, v_{liq} = 15 ml/s, $T_{liq.o}$ = 253K

p_{tot}, kPa	c_{HO2-}, mol/l	d, mm	U_{Cl2}	Y_D	T, K	p_w/p_{O2}
36	5	20	0.88	0.7	306	0.46
36	8	20	0.98	0.82	308	0.44
76	5	20	0.74	0.68	301	0.20
76	8	20	0.95	0.74	312	0.28
76	5	15	0.85	0.7	307	0.25
76	8	15	0.98	0.8	312	0.26

Although the ratio p_w/p_{O2} is relatively high, estimated $O_2(^1\Delta)$ loss due to I* quenching by water was less than 5% for $p_w/p_{O2} < 0.3$, provided that $O_2(^1\Delta)$ is mixed with atomic iodine downflow the supersonic COIL nozzle.

2.2.2. Modeling of the centrifugal separator

For the device designing, a number of impactor holes N_i and their diameter d_i was determined for given flow rates and permissible pressure drop Δp_i by the relation [6]

$$d_{d50} = 3\mathrm{Stk}_{50}^{1/2}\left(\frac{2h_G}{r_G C_C}\right)^{1/2}\left(\frac{\dot{V}_G+\dot{V}_L}{p\,N_c N_i}\right)^{1/4}\left(\frac{x_i r_M}{2\Delta p_i}\right)^{3/8} . \qquad (1)$$

By this equation, the design should prefer more holes with smaller diameter to less holes of larger diameter of the same total area.
A theoretical analysis was performed for the main generator parameters in **Table 3**.

Tab. 3
Input data for the separator model calculations

Gas input	Cl_2/He mixture 1 : 4
Total gas flow rate	n_{tot} = 115 mmol s^{-1}
Diffusion coefficient of Cl_2 in gas	D_{Cl} = 1.04 x 10^{-4} m^2 s^{-1}
Spray temperature	T = 260 K
Spray droplet diameter	d = 20 μm
Initial HO_2^- concentration in BHP	c_{H02-} = 8 M (kmol m^{-3})
BHP flow rate	V_L = 15 cm^3 s^{-1}
Total pressure	37.5 kPa (280 Torr)
Reactor volume	54 cm^3
Gas/liquid retention time in reactor	8 ms
Cl_2 utilization	0.98
BHP utilization	0.38
$O_2(^1\Delta)$ yield	0.82

By detailed calculations presented in the Reports of this Contract, a number of the holes N_i = 29 with diameter d_i = 3 mm was thus suggested to keep also a pressure loss at the impactor to 0.8 kPa. By this theoretical design, 50% of 2.3 μm-droplets and 99% of 3.2 μm-droplets should be separated from gas in this impact part of the centrifugal separator.

Finer droplets remaining in the gas should be removed in two separator slits, each of the height H, width a, and rectified length L (see Fig. 2). These droplets would be mostly smaller than ~3 μm (as calculated above). It is supposed that a liquid film of thickness h covers only outer surface of the slit. For calculations a coordinate system (x, y) was introduced, where the axis x is the rectified distance from the slit inlet and the axis y is perpendicular to the slit ($y = 0$ at the wetted surface, $y = h$ at the g/l interface, and $y = H$ at the dry surface). Droplet trajectories during their motion along the slits were computed by means of the hydrodynamic theory [6]. **Figs. 7a, b** illustrates examples of computed droplet trajectories for three droplet diameters and two separator rotation speeds. These trajectories give information about a length of the separator slit for certain droplet diameters at a certain separator rotation rates, provided that 90% separation efficiency of the impact separation is attained.

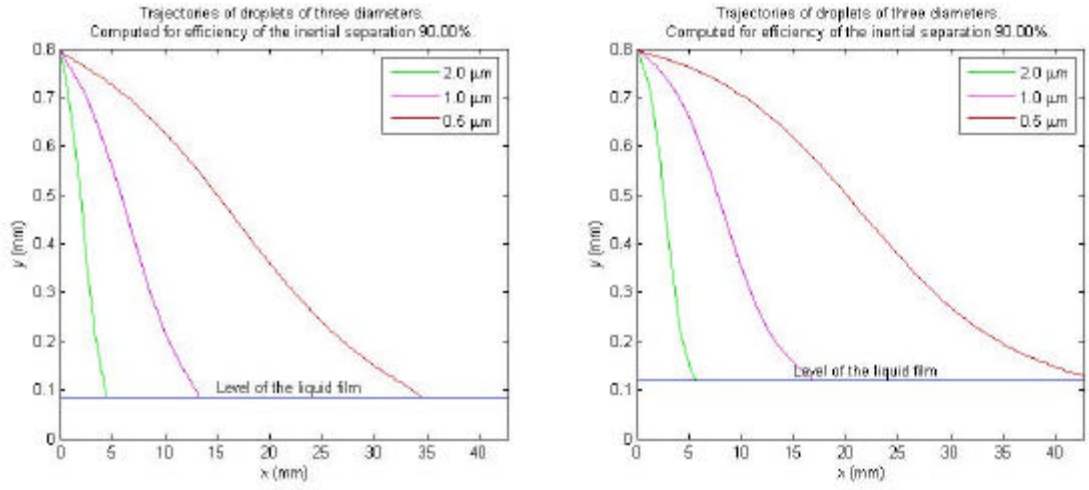

a) **b)**

Fig. 7. Computed droplet trajectories for three droplet diameters, and two separator rotation speeds: (a) 10,000 r.p.m., and (b) 5,000 r.p.m.

By these theoretical results, the BHP spray droplets with the diameter >0.5 μm should be entirely separated at the separator revolutions higher than 5,000 r.p.m. A pressure drop (Δp) in the separator depends also on revolution speed and efficiency of the impact separation: Δp = 1.95 kPa was calculated for 5,000 r.p.m. and 90% efficiency, which is ~5% of the generator pressure.

The theoretical analysis further showed that a major $O_2(^1\Delta)$ loss in the separator is caused by the pooling and quenching reactions in the gas phase. The 82% $O_2(^1\Delta)$ yield at the separator rotor slit inlet should be reduced to 69% only at the generator exit.

The results of mathematical modeling showed:

- **Enough high chlorine utilization (75–95%) and very high BHP utilization (36–54%) can be attained at realistic flow rates of BHP liquid and Cl_2 gas (Cl_2/He mixture 1:4) by using the commercial nozzle SAM-05-03 for the spray generation with droplets of ~20 mm in diameter.**

- **Sufficiently high $O_2(^1D_g)$ yield (up to 0.8) can be attained at $O_2(^1D_g)$ partial pressure of 5.5 kPa (40 Torr) during a very short time (5 ms).**
- **Efficient separation of liquid from gas can be realized by two-step process employing the centrifugal force, first the separation of larger droplets (>3 mm) by impact on the rotor wall, and then of finer droplets (>0.5 mm) in two slits in the rotor body at the rotation speed higher than 5,000 r.p.m.**

Detailed description of this theoretical research was presented in Reports of this Contract during the Research Phase 1 [10-13], and also given in [7, 8].

These theoretical results were heartening propositions for designing the CentSpraySOG device and experimental investigation of the generator operation.

3. Summary of progress in experimental investigations

3.1. Evaluation of the spray properties

A droplet size in the spray and a shape of the spray cone generated by the SAM-type nozzles in ambient atmosphere at different gas and liquid pressure at the nozzle inlet were studied first from the camera records and then by a precise laser-based diffraction method (SprayTec, Malvern Co., England) making possible to evaluate continuously a droplet diameter, droplet size distribution, and specific surface area of the spray. These measurements were performed due to inconvenient BHP properties first with the water spray and then with the BHP-like model liquid spray (70% glycerol-water mixture) having very similar physical properties (viscosity 18–23 mPas and surface tension 66.5 mN/m) at room temperature like 7.5 M-BHP solution at –20°C. Pressurized nitrogen was used as the atomizing gas. **Fig. 8** shows the set-up of these experiments. An example of measured droplet size distribution in the glycerol spray in dependence on the gas pressure introduced into the nozzle is shown in **Fig. 9**.

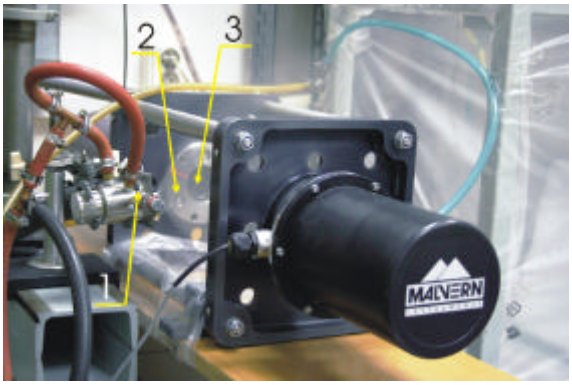

Fig. 8. Set-up of droplet size measurements by SprayTec
1–nozzle SAM-type, 2–spray, 3–detector input

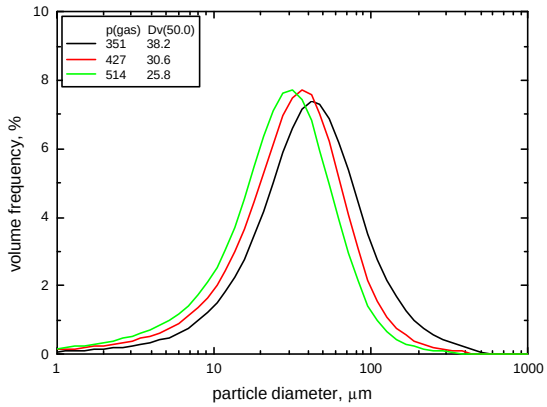

Fig. 9. Droplet size distribution in glycerol spray at different gas pressure. P_{liq} = 144 kPa, *x*=65 mm (x – distance from nozzle exit)

It was found that the droplet diameter (median of droplet diameter Dv(50)) decreased nearly linearly with increasing gas pressure introduced into the nozzle. In the range between 350 kPa and 600 kPa the median decreased from 40 μm to 15 μm. A liquid input pressure between 140 kPa and 200 kPa did not affect the droplet size distribution. At higher liquid pressure the droplets were larger (**Fig. 10**).

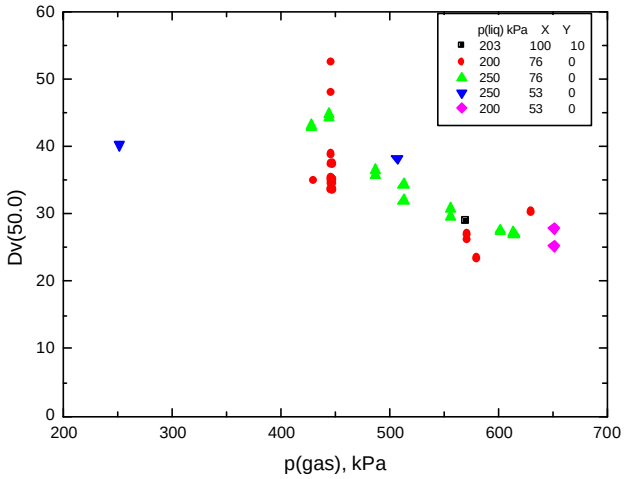

Fig. 10. Median of droplet diameter of glycerol in dependence on inlet nitrogen pressure. Nozzle SAM-05-03, P_L = 200 – 250 kPa, *x* = 53 mm, 76 mm, and 100 mm

The results of study of the spray properties showed:

- **Purchased commercial spray nozzle SAM-05-03 (BETE Fog Nozzle, Inc., MA) should satisfy requirements for the spray generation from very viscose BHP liquid.**
- **Input gas and liquid pressure into the nozzle, and flow conditions were optimized so that would provide the BHP spray with droplets of around 20 mm.**

Detailed description of this experimental research was presented in Reports of this Contract during the Research Phase 1 [10-13], and also given in [8, 9].

These supporting experimental results were fully transferred into a design of the spray singlet oxygen generator for study of $O_2(^1D)$ generation.

3.2. Singlet oxygen generation in the spray SOG

$O_2(^1\Delta)$ generation in the BHP/Cl_2 spray system was first studied in a stationary device without employing the centrifugal separation of liquid from gas exiting the generator. A main part of the device was a stainless steel rectangular reactor with removable top plate functioning as a holder of the spray nozzle. The inner reactor cross-section was 5cm x 5cm, and 16.2 cm long was a path of the spray. The reactor was equipped with two opposite glass windows (5cm x 3cm). The Cl_2/He gas mixture and the BHP liquid (cooled to -15°C to -20°C) was introduced into the two-phase spray nozzle at defined flow conditions to form required reaction spray. The device is partly shown in **Fig. 11**.

Fig. 11. Device with stationary spray $O_2(^1?_g)$ generator, equipped with two-phase spray nozzle SAM-type in reactor top. Red emission of $O_2(^1?_g)$ dimolar reaction observable in reactor window.

Quantitative measurements of $O_2(^1?_g)$ concentrations in the spray was based on the fundamental emission at 1268 nm using the Ge photodiode. The $O_2(^1?_g)$ emission was collected from a conical space in the reactor volume through the reactor window. In spite of very precise calculation of $O_2(^1?_g)$ concentrations from these records, these values were obviously partly distorted by diffraction and refraction of emitted radiation on the droplet surfaces. Pressure and temperature in the generator was also recorded on line by PC data acquisition system.

Figs. 12a, b gives example of results obtained during this investigation, showing dependences of the $O_2(^1\Delta_g)$ partial pressure on the total pressure in generator. The photodiode was centered in the axis of reactor window, i.e. 45.8 mm from the spray nozzle exit. The generator pressure was varied with a valve throttling the gas flow at the reactor outlet. The $O_2(^1\Delta_g)$ partial pressure attained a value up to nearly 4 kPa (~30 Torr) at the generator total pressure ~70 kPa (520 Torr). The evaluated $O_2(^1\Delta_g)$ partial pressure, P_Δ, was further utilized for evaluation of product of the chlorine utilization and $O_2(^1\Delta_g)$ yield, $U_{Cl}Y_\Delta = (x + 1)\, P_\Delta/P_{tot}$, where x is the dilution ratio of chlorine, n_{He}/n_{Cl2}, introduced in the nozzle (see chap. 4.2.). **Fig. 12b** shows an example of dependence of $U_{Cl}Y_\Delta$ on the total generator pressure measured in the pressure range of 10-80 kPa (75-600 Torr). In this series nitrogen was inlet into the nozzle as the fan gas, which extended the spray cone and so cleaned the window of $O_2(^1?)$ diagnostic cell.

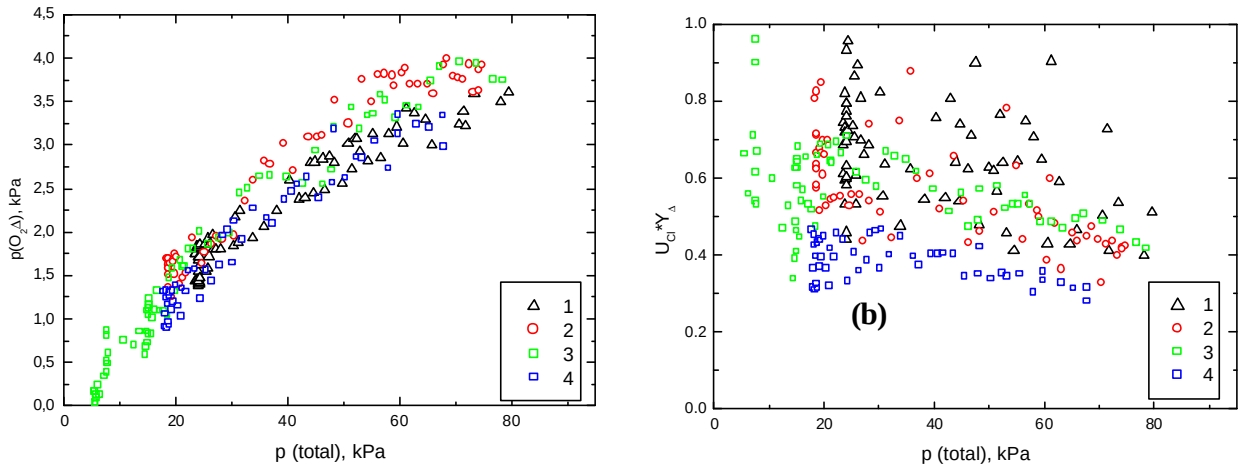

Figs. 12a, b. Dependence of the $O_2(^1\Delta)$ partial pressure **(a)** and the product $U_{Cl}Y_\Delta$ **(b)** on generator pressure. Gas flow rates (in mmol s^{-1}): 15 Cl_2 + 100 He + 46 N_2 (curve 1); 20 Cl_2 + 60 He + 60 N_2 (curve 2); 20 Cl_2 + 80 He + 60 N_2 (curve 4), 24 Cl + 80 He + 54 N_2 (curve 5); v_{BHP} = 12.6 ml/s (curve 1), v_{BHP} - 10.5 ml/s (curves 2 - 4).

The results of detailed parametric study of the spray singlet oxygen generator showed:

- **The $O_2(^1D)$ partial pressure was increasing with increasing total pressure in the generator, up to 70–90 kPa (520–680 Torr).**
- **A parameter $U_{Cl}Y_D$ (product of Cl_2 utilization and $O_2(^1D)$ yield) used for the SOG efficiency evaluation attained high values (up to 0.8) within very short contact time of 6-12 ms between gas and liquid phases. This coincided with results of modeling.**
- **The estimated BHP utilization was high (~40%) at the tested conditions; it was higher by one-two orders than in a jet-type SOG operating with a single BHP pass.**

Detailed description of this research was presented in Reports of this Contract during the Research Phase 1 a 2 [14-17], and also given in [8, 9].

These supporting experimental results were very important for the following research on originally designed and constructed the spray generator with a centrifugal separation of liquid and gas phases.

3.3. Research on the centrifugal spray generator

3.3.1. Design and construction of the CentSpraySOG

The device was constructed by the original design and technical drawings elaborated on the base of the modeling and experimental results described above. This prototype generator should drive a 500W-high-pressure supersonic COIL.

The overall CenSpraySOG hardware is shown in **Fig. 13**. The main components, i.e. the rotating separator with cylindrical reaction cavity inside, and the rotor shell with two slits and distributing rotor flange are shown in **Fig. 14.**

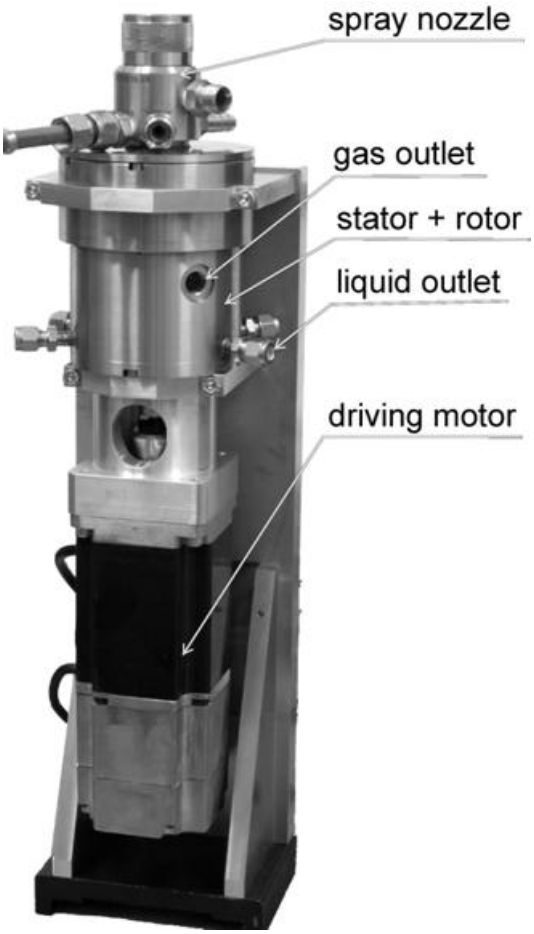

Fig.13. CentSpraySOG as a whole device

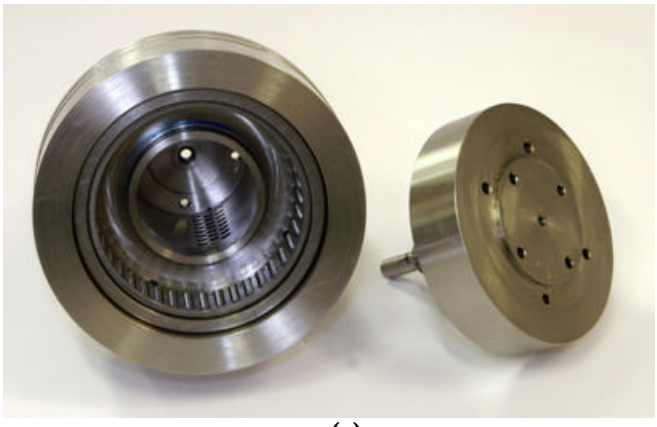

(a)

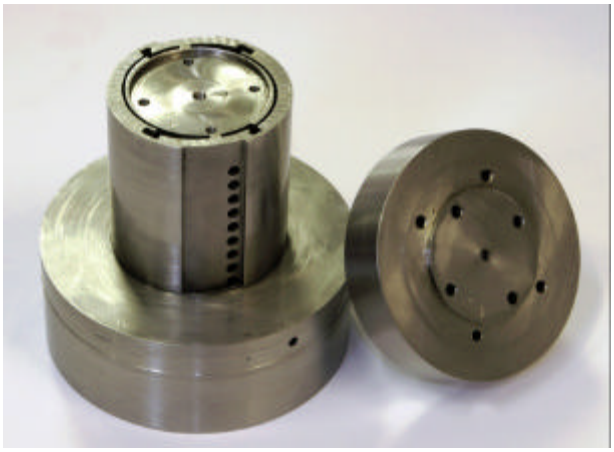

(b)

Fig.14. Rotating separator with cavity inside (a), and rotor with slits and distributing rotor flange (b)

Final version of the rotor was fabricated with parameters given in its cross-section in **Fig. 15.**

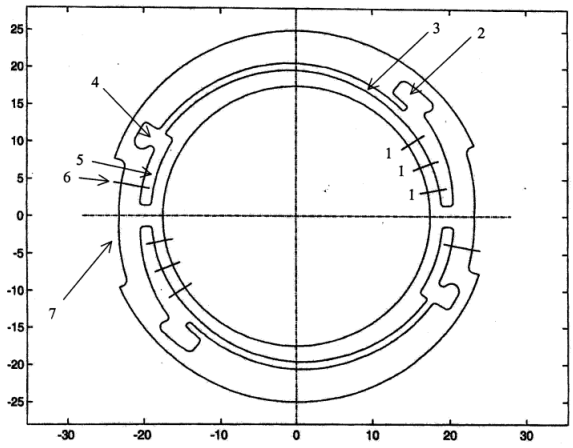

Fig.15. Cross-section of the separator rotor (scale in mm). 1 – holes for spray input into the rotor shell. 2 – channel for collection of BHP separated by impact, 3 – slits for separation of remaining droplets by the centrifugal force, 4 – channel for collection of BHP separated by the centrifugal force, 5 – channel for collecting gas, 6 – holes for gas exit, 7 – grooves for transport of exiting gas

Two narrow slits 3 in the rotor shell are 1 mm high, 50 mm wide, and 37 mm long. Their shape was described by the equation

$$q = q_{in} - \tan\alpha_{in} - \arctan(1/\tan\alpha_{in}) + (r^2 - 1)^{1/2} + \arctan(1/(r^2 - 1)^{1/2}) \qquad (2)$$

where the polar angle q is a function of the radial coordinate r. Symbols q_{in}, α_{in}, and r_{in} relate to respective parameters at the inner radius of the slit. Here r is a dimensionless radial coordinate

$$r = r/q\,, \qquad (3)$$

where
$$q = r_{in} / (1 + \tan^2\alpha_{in})^{1/2} \qquad (4)$$

The angle between the slit tangent and radial coordinate is

$$\alpha = \arctan(r^2 - 1)^{1/2}\,. \qquad (5)$$

The length of the channel contour between radii r_{in} and r is

$$L(r) = (r^2 - r_{in}^2) / 2q\,. \qquad (6)$$

The fabrication of the slits, collecting channels 2, 4, 5, three rows of 3 mm-holes for the spray entrance in the separator wall ((29 holes at each channel input) were made by a computer controlled electro-erosive machining in the specialized workshop. Nine 3 mm-holes 6 were drilled in one row for the gas outlet from the separator rotor. Two grooves 7 on the outer rotor surface of calculated profiles serve as ducts for exiting gas.

The body of the stator was made of stainless steel. Two separator rotors were tested, made of stainless steel and titanium, to prove the effect of theoretically known less $O_2(^1\Delta)$ quenching on the titanium surface.

For driving the separator rotor, three types of motors were employed subsequently. The motor Maxon, type MO60237, 85W (Switzerland) with the rotation speed up to 7000 r.p.m. was too weak for the centrifuge operation on account of friction losses on Viton sealing rings. The second motor Omron, type R7M-A75030, 750W (Japan) was adequately powerful but it operated at the highest rotation speed 4000 r.p.m. The later experiments with BHP/Cl_2 chemistry for the $O_2(^1\Delta)$ generation showed that a higher rotation speeds of the separator rotor should be employed for a more efficient gas-liquid separation. Therefore still more powerful motor (type ABB Servomotor SDM631-012N0-140 with a frequency converter ACS550) providing a rotation speed up to 10 000 r.p.m motor was employed for driving the separator rotor.

The device of CentSpraySOG has undergone through many constructional modifications during the research on this contract followed from some unexpected problems that emerged only during experiments. These modifications are described in details in the previous interim reports and documented in technical drawings involved in them.

3.3.2. Experimental set-up for investigation of the CentSpraySOG

A scheme of the set-up involving gas and liquid management and a photo of the main device part are in **Fig. 16.**

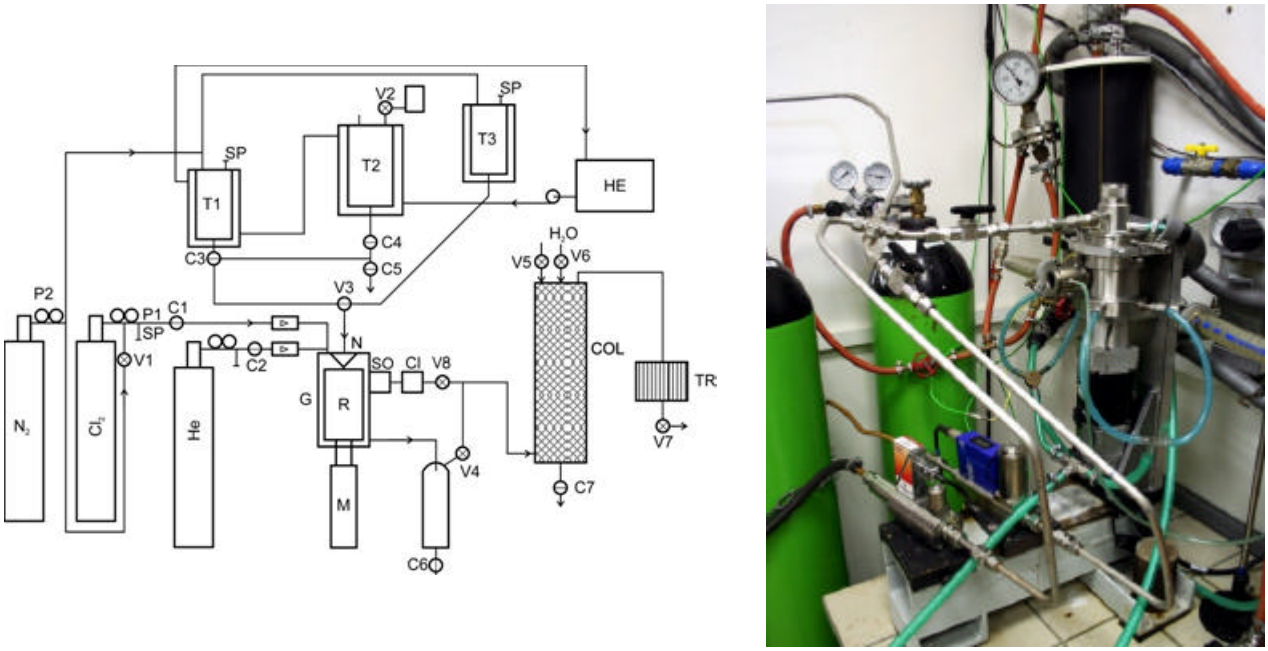

Fig.16. Experimental set-up with the centrifugal spray $O_2(^1\Delta)$ generator (description in the text)

A two-phase spray nozzle *N* with external gas-liquid mixing (type SAM-05-03) was used in most experiments for the BHP spray formation. The nozzle was tightly fixed in the top of generator-reactor body *G*. Chlorine was introduced into the nozzle from a 40-liter pressurized gas cylinder through the pressure reducer *P1*, cock *C1*, and mass flow regulator (M+W Instruments GmbH, Germany, type

D-6251/8mm-SS). A safety piping *SP* prevented an over-pressuring in the chlorine line. A parallel gas line with the pressure reducer *P2*, cock *C2*, and mass flow regulator (Bronkhorst, Netherlands, type F-202AC-FBB-44-V) served for He management. He and Cl_2 flows were mixed in different ratio in the spray nozzle entrance. The N_2 management with valve *V1* was used for scavenging the Cl_2 line after experiments ending. BHP liquid pressurized by nitrogen in a cooled stainless steel tank *T1* was introduced into the spray nozzle. The BHP solution with a resulting HO_2^- concentration of 5.3 M (mol/dm^3) was prepared in a jacketed mixing tank *T2.* The jacket tanks were cooled to (-20±3) °C by glycol-water mixture circulating between these tanks and heat exchanger *HE* cooled by a 2kW-refrigerating aggregate. The BHP temperature in both tanks was measured by jacketed NiCr-Ni thermocouples. A residual BHP in both tanks was drained after experiment finishing by the cock *C4*, three-way cock *C3*, and cock *C5*. The tank *T3* served as a distilled water reservoir for rinsing the device. The gas and BHP lines were made of stainless tubes of 10 mm o.d. equipped with fittings Swagelok (Solon, OH, USA). Singlet oxygen in the gas exiting CentSpraySOG device was detected in the optical cell *SO* by Ge photodiode (Judson Technologies, LLC, PA, USA, type J16-5SP-R05M-SC), and residual chlorine in optical cell *Cl*. The gas was exhausted by the rotary pump ($300 m^3/h$) through the column *COL* and LN_2 trap *TR.*

Much attention was paid to the $O_2(^1D)$ optical measurements from the point of detection cell configuration. A fast $O_2(^1\Delta)$ quenching at high partial pressures generated by the CentSpraySOG and non-uniform gas flow in the cell for $O_2(^1\Delta)$ detection can cause a non-homogeneous distribution of $O_2(^1\Delta)$ concentration in the cell. The first cell used in initial period of the generator testing was tightly closed to the generator exit and the $O_2(^1\Delta)$ radiation was collected from the inner volume of frustum shape. In order to prove it, a 2-D simulation of the reactive flow inside the optical cell was performed. A decrease in the singlet oxygen concentration by quenching depends on the $O_2(^1\Delta)$ partial pressure and residence time in the cell. Therefore, seven cases for different partial pressures of $O_2(^1\Delta)$, total flow rate and total pressure (i.e., a different residence time) were modelled. For simplicity, 100% chlorine utilization was assumed in all cases. After a converging each simulation, the integral was calculated

$$\mathrm{I} = \int c_{\Delta}(R, f)\frac{\cos j}{R^2}\, dj\, dR dA \qquad (7)$$

The integration is given over an angle of deflection, j, a distance of the simulation element centre from the photodiode, R, and over a simulation element area, A. A light flux hitting the photodiode surface and also the photodiode current are directly proportional to a value of the integral I. We assumed previously that the $O_2(^1\Delta)$ concentration in the optical cell for evaluation from its partial pressure is quite uniform, and so it corresponds to the value $c_{\Delta,in}$ in gas exiting the generator. Then the integral in (7) can be evaluated as

$$\mathrm{I}_{\mathrm{unif}} = c_{\Delta,in}\int \frac{\cos j}{R^2}\, dj\, dR \qquad (8)$$

The ratio I_{unif}/I determines a factor, by which we have to multiply the values of $O_2(^1\Delta)$ partial pressure measured in the cell in order to obtain the values of $O_2(^1\Delta)$ partial pressure in gas at the CentSpraySOG exit. One example of the simulation results for is shown in **Fig. 17** illustrating velocity vectors coloured by the $O_2{}^1(\Delta)$ mass fraction. A large vortex structure with low $O_2(^1\Delta)$ concentration is obvious from this Figure in the vicinity of the photodiode. This region significantly contributes to the integral (8).

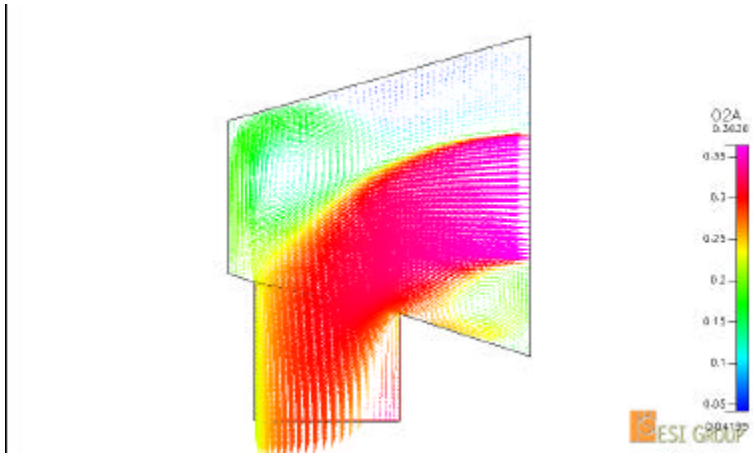

Fig. 17. Velocity vectors coloured by $O_2(^1\Delta)$ mass fraction. Gas inlet into the cell from the right side (violet colour). Flow rates, mmol.s^{-1}: 20 mmol/s Cl_2, 60 mmol/s He; P_{total} = 50 kP; $P_{\Delta,inlet}$ = 6.25 kPa

This modeling involving the $O_2(^1\Delta)$ loss in the used optical cell showed that $O_2(^1\Delta)$ concentration in it was rather non-homogeneous and the measured values were not quite correct. Based on this finding, a new detection cell was designed and fabricated and used in the next further experiments. The gas flow through this cell is direct, nearly without a "dead" spaces in it, where whirls could be formed resulting in additional $O_2(^1\Delta)$ loss. Improved homogeneity of the $O_2(^1\Delta)$ concentration in this newly designed cell shown in **Fig. 18** was proved.

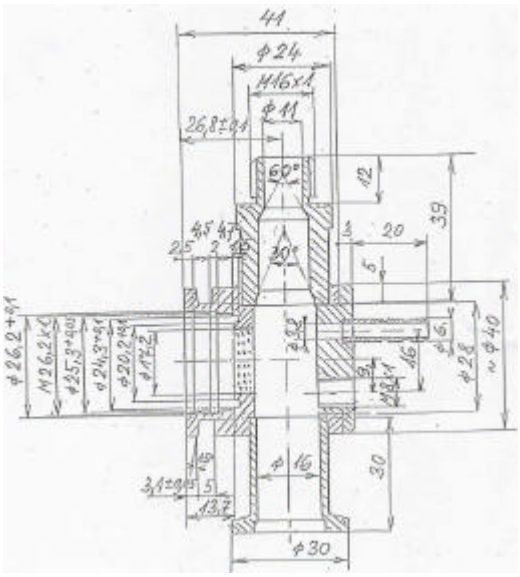

Fig. 18. Technical drawing of the new $O_2(^1\Delta)$ optical cell

Germanium photodiode was used with the active size of 5 mm in diameter and responsivity of 0.6 A/W for the 1.27 μm wavelength (Judson Technologies, LLC, PA, USA, type J16-5SP-R05M-SC). A commercial preamplifier with a gain of $1x10^7$ V/A was employed (type PA-7-70, Judson Technologies, LLC, PA, USA). The emitted light was filtered by means of the interference filter with 53.2% transmission at 1.27 μm (CVI Laser LLC). The calibration constant, k_Δ = 3047 Pa/V, determining a relation between the $O_2(^1\Delta)$ partial pressure and output voltage of the photodiode current amplifier was calculated for temperature 315 K and the given optical cell geometry, filter transmission, and diode responsivity.

3.3.3. Calculation of heterogeneous $O_2(^1D)$ loss on channel walls in the separator

In singlet oxygen generation a heterogeneous $O_2(^1\Delta)$ quenching on the walls of gas channels in the rotating separator of CentSpraySOG can be a problem. We therefore made a theoretical estimation of $O_2(^1\Delta)$ loss in the reaction space and transport channels. Main quenching processes are:

(i) homogeneous dimolar pooling and self-quenching reactions

$$O_2(^1\Delta) + O_2(^1\Delta) \rightarrow O_2(^1\Sigma) + O_2(^3\Sigma), \qquad k_{10} = 2.7x10^{-17}\ cm^3/s, \qquad (10)$$

$$O_2(^1\Delta) + O_2(^1\Delta) \rightarrow O_2(^3\Sigma) + O_2(^3\Sigma), \qquad k_{11} = 1.7x10^{-17}\ cm^3/s, \qquad (11)$$

(ii) heterogeneous $O_2(^1\Delta)$ quenching on channel walls

$$O_2(^1\Delta) + \text{wall} \rightarrow O_2(^3\Sigma) + \text{wall} \qquad \gamma_{12} \qquad (12)$$

The process (12) takes place predominantly in two narrow slit channels inside the rotating separator where smaller BHP droplets are separated by the centrifugal force. A slit is 1 mm high but during the separation process outer slit wall is covered with a liquid film so the gas can theoretically flow through the slit in a space corresponding to 0.8 mm (calculated for the rotation speed 4000 r.p.m.). Simplified kinetic equations were employed for calculation of the $O_2(^1\Delta)$ deactivation on the walls of two spiral slit channels and also the homogeneous $O_2(^1\Delta)$ loss in all gas spaces of the separator. A wall accommodation (deactivation) coefficient for the used stainless steel $g = (3.4 \div 6.4)x10^{-3}$ was considered. It was shown during these calculations that the mass transfer coefficient k_d in gas is much higher than the coefficient corresponding to a wall loss, gu_t = 0.739 m/s, where u_t is the thermal velocity of oxygen molecules, (the upper limit for the coefficient $g = 6.4x10^{-3}$ was considered). So we neglected diffusion restrictions and evaluated the heterogeneous loss from the equation

$$\frac{dc}{dt} = \frac{-gu_t}{h}c, \qquad (13)$$

where h is the diffusion path. The homogeneous loss in the reactions (10) and (11) was calculated by integration of the equation

$$\frac{dc}{dt} = -k_p c^2, \qquad (14)$$

with k_p = 36.7 m^3/mol/s (= 6.1 x 10^{-17} cm^3s^{-1}). This modeling was presented in details in the interim [4], and pointed out a significant heterogeneous $O_2(^1\Delta)$ quenching in the narrow slit channels of the stainless steel separator rotor due to a high $O_2(^1\Delta)$ quenching (accommodation) activity of iron and other steel components.

The above estimations prompted us for fabrication of the separator rotor made of titanium. This material has much lower $O_2(^1\Delta)$ quenching (accommodation) coefficient ($\gamma_{Ti} = 6.5 \times 10^{-5}$), and is also corrosion resistive.

For a more precise estimation of the heterogeneous $O_2(^1\Delta)$ loss on the slit walls, 2-D calculations were also performed. The 2-dimensional stationary diffusion equation (15) was solved to evaluate $O_2(^1\Delta)$ quenching on both slit walls, the inner metal wall and the outer slit wall covered with a BHP film.

$$\frac{\partial c}{\partial t} = 0 = D\frac{\partial^2 c}{\partial y^2} - u_x \frac{\partial c}{\partial x} \tag{15}$$

with the boundary conditions

$$J(y=0) = D\frac{\partial c}{\partial y}\bigg|_{y=0} = g_{BHP} v_t c(y=0) \tag{15a}$$

$$J(y=H) = -D\frac{\partial c}{\partial y}\bigg|_{y=H} = g_{wall} v_t c(y=H), \tag{15b}$$

where c is the molar concentration of $O_2(^1\Delta)$, g is the quenching coefficient on the wall and BHP, respectively, v_t is the thermal velocity of oxygen molecules, x is the coordinate along the channel length, and y is the distance from the BHP level. The boundary $y = 0$ corresponds to the BHP surface, and $y = H$ corresponds to the inner (metal) wall. The correct formula for the diffusion coefficient of oxygen in helium is

$$D = 0.001103\frac{T^{3/2}}{p\left(\frac{1.0260}{T^{0.08742}} + \frac{13.28}{T^{0.8491}}\right)}. \tag{16}$$

Blauer *et al.* [4] used in their model the quenching probability of $O_2(^1\Delta)$ on the BHP surface, γ_{BHP}, in the range of $2\text{x}10^{-3} - 5\text{x}10^{-4}$ to fit the calculations to their experimental results. We also consider these two boundary values of γ_{BHP} in our calculations. The results of the performed modeling were given in are shown in **Table 4.**

Tab. 4

$O_2{}^1(\Delta)$ loss(in %) at different pressures and loss probabilities

$P_{cent,tot}$, kPa	23	46	58
P_{Cl2}, kPa	5	10	12.5
$U_{Cl}Y_?$, %	58	41	34
wall loss, 1-D, stainless steel	17.6%	32.2%	38.8%
wall loss, 2-D, steel+BHP ($\gamma = 5\text{x}10^{-4}$)	16.7	25	28.6
wall loss, 2-D, titan+BHP ($\gamma = 5\text{x}10^{-4}$)	1.7	3.4	4.3
wall loss, 2-D, BHP+BHP, ($\gamma = 5\text{x}10^{-4}$)	3.1	6	7.6
wall loss, 2-D, BHP+BHP, ($\gamma = 2\text{x}10^{-3}$)	11.2	20.3	24.4

This 2-D calculation resulted in $O_2(^1\Delta)$ losses lower than gave results of former 1-D calculations; a difference between them was larger for higher pressures considered. The calculated $O_2(^1\Delta)$ loss on titanium surface (the sixth row in Table 4) were substantially lower than for stainless steel. There is however possible that a thin BHP film covers both walls of the slits, which would avoid the effect of the constructional material. The results considering this case (both walls with BHP film) are given in the last two rows of Table 4, for lower and upper bound for γ_{BHP}.

3.3.4. Measurement of chlorine utilization

A great effort was devoted to evaluation of a content of the residual chlorine in generated singlet oxygen. Two different instruments were used for measurements of the Cl_2 concentration by absorption spectrometry. The spectrophotometer Spekol 1200 (Analytic Jena AG, Germany) with the polychromator and diode array analyzed the collected spectrum in the region of 200-740 nm. The second instrument was the spectral photometer Spectrum 10 manufactured for our laboratory order (Unilab Co., CR). A monochromatic light passed through a cell with 4.6 cm long active path, located downstream of the $O_2(^1\Delta)$ detection cell (see Fig. 19). The light beam was perpendicular to the gas flow direction. The light passing the cell was filtered with the band pass filter UG1 (Carl Zeiss Jena, Germany) transmitting light between 300 nm and 400 nm.

A measurement of the residual chlorine concentration by absorption spectroscopy was fairly complicated problem in the studied system. In all measurements with the $O_2(^1\Delta)$ generation the light transmission passing the detection cell continually decreased, as can be seen in one experimental example shown in **Fig. 19.**

This record was taken with the spray nozzle SAM-06-04 and at a rotor speed of 9000 r.p.m. In this experiment BHP foam was entrained with gas into the detection cell at 175 s. A transmission jump observed at 53 s corresponded to light absorption with chlorine (σ_{400nm} = 1.8 x 10^{-20}cm^2), the transmission increase at 70 s was due to a drop-off chlorine concentration due to reaction with BHP introduced into the generator. A transmission variation between 53 s and 70 s was caused by a variation of the Cl_2 flow rate caused by improper function of the flow controller. A transmission decrease between 70 s and 175 s was caused very probably by settling of fine BHP droplets on windows of the optical cell. An increase in the He flow rate from 90 mmol/s to 160 mmol/s at 120 s had no remarkable effect on the light transmission. When BHP was atomized with helium only or only chlorine with helium without BHP was introduced into the spray nozzle, no decrease in the light transmission was observed. The observed temporal decrease in transmission was faster for light of shorter wavelength (250–350 nm) than for 400 nm light. We deduce from this finding that effect of aerosol droplets (possibly also their amount) increases with their decreasing size.

The described problem with evaluation of the residual chlorine forced us to evaluate it from spectra measured by Spekol 1200 in the wavelength range of 300 nm – 500 nm. Such spectra recorded in the same experiment run as described in Fig. 22 are shown in **Fig. 20**. Concentration of the residual chlorine was evaluated from a difference between the measured transmission and the background transmission. This background was obtained by a linear approximation passing through curves in the

regions, where chlorine absorption can be neglected, i.e. 250–265 nm, and 465–500 nm. Absorption cross section of chlorine is given in **Table 5**.

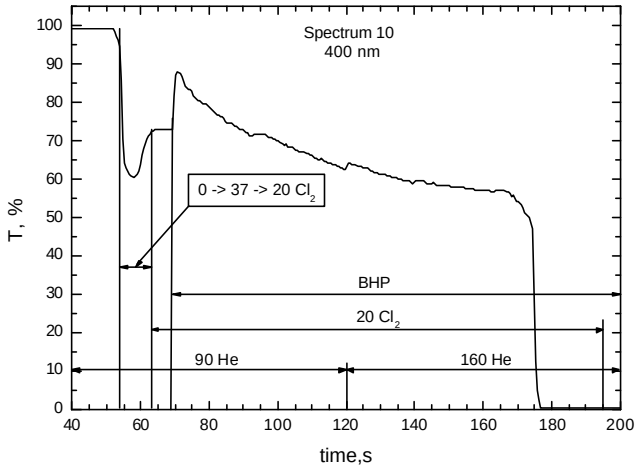

Fig. 19. Time course of 400 nm light transmission through detection cell of the photometer Spectrum 10.

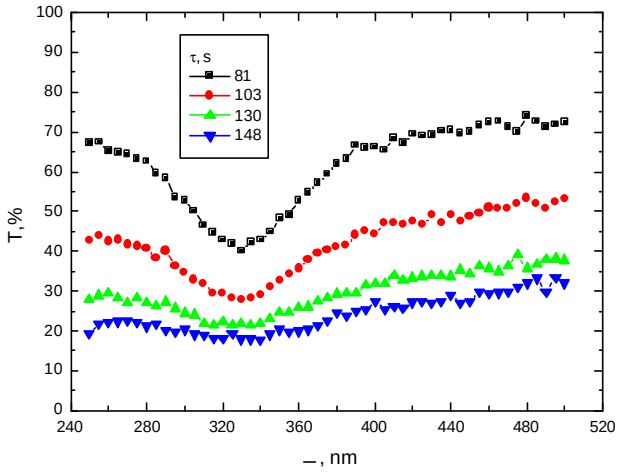

Fig. 20. Time change of spectra measured with Spekol 1200. τ is time from the experiment start.

Gas flow rates (in mmol/s): (0→37→20) Cl_2 + 90 He (53 s - 63 s),
20 Cl_2 + 90 He (63 s – 120 s), and 20 Cl_2 + 160 He (120 s – 195 s), v_{BHP} = 14 - 17 ml/s (70 s – 205 s),

It was found that the transmission difference obtained by this procedure was nearly directly proportional to the absorption cross-section of chlorine.

Tab. 5
Absorption cross section of chlorine (298 K)

λ, nm	**10^{20} σ, cm^2**	**λ, nm**	**10^{20} σ, cm^2**
260	0.20	370	8.4
270	0.82	380	5.0
280	2.6	390	2.9
290	6.2	400	1.8
300	11.9	410	1.3
310	18.5	420	0.96
320	23.7	430	0.73
330	25.5	440	0.54
340	23.5	450	0.38
350	18.8	460	0.26
360	13.2	470	0.16

The curves in Fig. 23 demonstrate a temporal decrease in transmission, which is most probably due to settling of fine BHP aerosol particles on the windows of detection cell. A size of these particles escaped from the separator at 9 000 r.p.m. should be smaller than 0.5 μm according to our calculations (see

chap. 2.2.2.). These very small droplets then scattered very effectively the light of wavelength shorter than 500 nm, which agreed with the recorded dependences in Fig. 23. Formation of the fine aerosol during the $O_2(^1\Delta)$ generation process occurred very probably by a similar mechanism as described by Whitefield *et al.* [21]. They measured density of the aerosol formed in the rotating disc generator and found that the size of particles was between 0.5 μm and 0.01 μm. They ascribed formation of this aerosol to a mechanical process of the explosion of gas bubbles on the BHP/Cl_2 interface.

It could be supposed that scattering effect of such aerosol (with particles <0.5 μm) on the COIL radiation (1.315 μm) driven by the CentSpraySOG will be minor than on light of shorter wavelength, and the observed effect of light scattering on particles settled on laser mirrors could be diminished by purging .

Chlorine concentration was calculated from the Lambert-Beer law

$$c_{Cl2} = ln\ (I_o/I) / (s\ \ l) \qquad (17)$$

where I is the transmission, I_o is the "background" transmission, and l is the light path-length in a cell.

An example of chlorine concentration dependence on wavelengths evaluated for several SOG operation times is shown in **Fig. 21**.

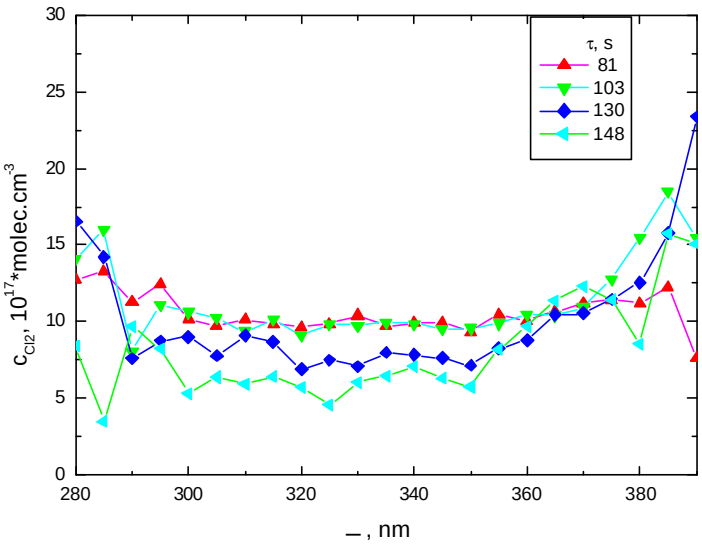

Fig. 21. Chlorine concentration calculated for different wavelengths. τ denotes time from experiment starting. The same experimental conditions as in Figs.22, 23

Curves in this figure illustrate that the evaluated chlorine concentration is nearly independent on the wavelength for the region of 300–350 nm The data are much more scattered outside this region, which is probably due to small differences between I_o and I, resulting in a larger error of the ratio I_o/I.

Chlorine utilization, U_{Cl}, was calculated from the relation

$$U_{Cl} = 1 - \frac{c_{Cl2(resid)}}{c_{Cl2(input)}} \quad (18)$$

where $c_{Cl2(resid)}$ is the mean residual chlorine concentration evaluated for the region 300–350 nm. The chlorine concentration at the generator input, $c_{Cl2(input)}$, was calculated as

$$c_{Cl2(input)} = \frac{n_{Cl2}}{n_{Cl2} + n_{He}} \frac{P_{gen} N_A}{RT} \quad (19)$$

where n is the molar flow rate, P_{gen} is the generator pressure, and N_A is the Avogadro constant.
The values of U_{Cl}, evaluated for given conditions and running times were equal to 0.708, 0.685, 0.675, and 0.682. They were nearly independent on the He flow rate, changed from 90 mmol/s to 160 mmol/s in 120 s. In other experiments, U_{Cl} was between 0.75 and 0.84 at 13–22 mmol/s Cl_2, 120 mmol/s He, and the generator pressure of 70 kPa. The concentration of the residual chlorine was from $3x10^{17}$ cm^{-3} to $6.7x10^{17}$ cm^{-3}. When the generator pressure was only 50 kPa, the U_{Cl} was lower (0.65) probably due to a shorter gas residence time in the reactor.

The design and development of the CentSpraySOG device, including the detection techniques underwent many successive modifications and improvements. They were supported by plenty of calculations, computational modeling, and gathered experience.

More details inclusive technical drawings were presented in Reports of this Contract [13-20], and some results were obtained recently.

This device was tested in many experimental sets. The results obtained by the end of this contract are summarized in the next chapter.

4. Most significant experimental results on the CentSpraySOG

4.1. Testing of separation efficiency

The first task solved on the new originally designed device of CentSpraySOG was investigation of the gas-liquid separation by the developed device (described in chapter 2). This investigation started with chemically non-reactive gas/liquid system first at atmospheric pressure in the generator and then at lower pressure (sub-atmospheric pressure), right to SOG operation with the BHP/Cl_2 chemistry at different gne generator pressures. Optimal gas and liquid flow conditions were searched to obtain the best separation. The rotation speed of the separator rotor was changed from 2000 r.p.m. up to 9000 r.p.m., rotors made of stainless steel and titanium were tested, and many technical improvements of the device and experimental set-up were performed during this study. The results are further given in a summary form

4.1.1. Centrifuge operation with non-reactive gas-liquid system at atmospheric pressure

First tests were performed with water and He. 80 mmol/s He as the atomizing gas and 11.6 ml/s of water under pressure (220 kPa abs.) was introduced through the nozzle SAM-05-03 into the

"reaction" space of the generator, where the water spray was formed at atmospheric pressure. A rotation speed of the separator rotor was 2000 r.p.m only, which resulted in penetration of some liquid into the outlet gas after ~20s–device operation. This finding required afterwards a few constructional rotor modifications.

Next tests were performed with model solutions having viscosity (17–18 mPas at 25°C) very similar to the BHP solution with 6–7 M HO_2^- at temperature typical for a SOG operation (–20°C). Two model liquids were used: 70% water solution of glycerol and 32% NaOH with a flow rate from 4.6 ml/s to 7.2 ml/s, respectively. Nitrogen with a flow rate 50 mmol/s was used as the atomizing gas. A rotation speed of the separator rotor was increased to 4000 r.p.m. These experiments proved enough smooth separator operation without liquid in the gas line (only a fine aerosol was visually observed in the exiting gas after several minutes of operation.

4.1.2. Centrifuge operation with non-reactive gas-liquid system at sub-atmospheric pressure

The same model liquid (32% NaOH solution) with a flow rate up to 10 ml/s, and the gas mixtures of He and N_2 were used in these experiments with 60 mmol/s He and up to 36 mmol/s N_2. A pressure in the spray reactor (generator), controlled by a throttling of the valve in the gas exit line varied from 25 kPa (~188 Torr) to 100 kPa (750 Torr). The separator rotated with the speed of 4000 r.p.m. No liquid droplets were observed in the gas exiting the separator under these operation conditions.

Somewhat worsening of liquid separation was observed when N_2 flow rate was increased to 50 mmol/s (at the same He flow rate of 60 mmol/s), and the generator pressure was decreased under 50 kPa. This effect of lower generator pressure resulted in a higher gas velocity in the separator gas channels, which caused entraining some liquid into the gas flow.

Further separation tests were performed with a less concentrated NaOH solution (9.7% w/w) having lower viscosity (1.84 mPas at 20°C), which is closer to the BHP viscosity at temperatures typical for the reaction space of our spray generator (30°C - 50°C). In these experiments the gas-liquid separation was effective (no droplets were visible in gas exiting the separator) at 60 mmol/s He and 17 mmol/s N_2, 12 ml/s NaOH, and generator pressures higher than 28 kPa (210 Torr). These flow and pressure conditions would suit also to $O_2(^1\Delta)$ generation in the CentSpraySOG. With the flow consisting of 60 mmol/s He and 42 mmol/s N_2 and the generator pressure less than 30 kPa some droplets were observed at the detection window.

4.1.3. Centrifuge operation with reactive BHP/Cl_2 system at sub-atmospheric pressures

The first experiments performed with the BHP and the He/Cl_2 mixture already signalized that this reaction system brings into the CentSpraySOG operation new phenomena that were not observed in experiments with the non-reactive systems. It resulted in worsening the efficiency of separation process at the flow and pressure conditions, at which it worked well with the BHP-like model liquids. Droplets and even foam were sometimes entrained with gas and observed on the window of the $O_2(^1\Delta)$ optical cell. We evaluated the separation process by observing droplets striking upon the window placed in the $O_2(^1\Delta)$ detection cell (instead of interference filter) and also from camera records. Much effort was devoted to solve this problem and searching for conditions that avoid this. Some results are given here.

Nearly no BHP droplets were observed on the window at 60 mmol/s He, 15 mmol/s Cl_2, and the generator pressures above 50 kPa (375 Torr). When the Cl_2 flow rate was increased to 27 mmol/s and $P_{gen} \leq 60$ kPa (450 Torr) some droplets were observed. Their entraining was partly suppressed by adjusting a pressure difference between the gas exit and the BHP exit attained by a throttling gas flow from the generator by the valve V8 with opened valve V4 in Fig. 19. This improved the separation at the flow rates up to 80 mmol/s He and 20 mmol/s Cl_2, and when the generator pressure was at least 35 kPa (~260 Torr). A higher gas flow rates or lower generator pressure resulted in worsening the separation efficiency. These experiments were performed with the driving motor enabling a maximum rotation speed 4000 r.p.m.

Further enhancing of the separation efficiency was solved by installing faster and more powerful motor. This decision was supported by our previous theoretical estimations, indicating that the centrifugal force was 6.25times higher for 10 000 r.p.m. than 4000 r.p.m. The motor ABB providing the rotation speed up to 10 000 r.p.m. was therefore purchased. In the experiments performed at 6000 r.p.m., and with 90 mmol/s He, up to 25 mmol/s Cl_2, and at the generator pressures higher than 50 kPa (375 Torr), the exiting gas was visually free of droplets. When He flow rate was increased to 160 mmol/s at 18 mmol/s Cl_2 some BHP droplets appeared in the gas, when the generator pressure was less than 45 kPa,.

The experiments described above were performed with the separator rotor made of stainless steel. We let fabricated the second separator rotor made of titanium. It should be advantageous for a much lower heterogeneous $O_2(^1\Delta)$ quenching on this metal than of stainless steel, AISI 316 used. The tests of the BHP decomposition on both metals showed that the BHP decomposition rate was too slow to form some foam during the separation. This was also proved in testing the separator efficiency with the Ti rotor because no significant improvement was observed.

4.2. Experimental study of $O_2(^1D)$ generation in the CentSpraySOG

4.1.1. Measurements with separator rotor made of stainless steel

The first sets of experiments with $O_2(^1\Delta)$ generation was performed on the CentSpraySOG device with the spray nozzle SAM-05-03, and the separator rotor made of stainless steel. During these studies, the overall efficiency of $O_2(^1\Delta)$ production was characterized by the product of the chlorine utilization, U_{Cl}, and the $O_2(^1\Delta)$ yield, $Y_?$ (the parameter $U_{Cl}Y_\Delta$) because we could measure the $O_2(^1\Delta)$ concentration only (and the $O_2(^1\Delta)$ partial pressure, P_Δ) but not a residual chlorine concentration in that period. The product $U_{Cl}Y_\Delta$ was calculated from the relation

$$U_{Cl}Y_\Delta = P_\Delta/(P_{Cl2(res)} + P_{O2}) \cong (x + 1)\, P_\Delta / P_{tot} \qquad (20)$$

that was developed by the following procedure. The total generator pressure, P_{tot}, equals to

$$P_{tot} = P_{He} + P_{Cl2(res)} + P_{O2} + P_{H2O} \qquad (20\text{-}1)$$

where the index $Cl_{2(res)}$ denotes the residual chlorine. The relation between P_{He}, $P_{Cl2(res)}$, and P_{O2} is given by

$$P_{He} = x\,(P_{Cl2(res.)} + P_{O2}) \qquad (20\text{-}2)$$

where x is the input He/Cl_2 ratio.
The total gas pressure then equals to

$$P_{tot} = (x + 1)\,(P_{Cl2(res)} + P_{O2}) + P_{H2O} \qquad (20\text{-}3)$$

P_{H2O} of BHP solution at a spray temperature between 30°C and 50°C ranges from 2.8 to 8.4 kPa, i.e. from 5% to 17% of P_{tot} = 50 kPa. In the experimental range of P_{tot} = 20–80 kPa, the water vapor pressure can be neglected, and so

$$P_{tot} \cong (x + 1)\,(P_{Cl2(res)} + P_{O2}) \qquad (20\text{-}3')$$

Cl_2 utilization, U_{Cl}, can be expressed as

$$U_{Cl} = n_{O2}/n^{o}_{Cl2} = n_{O2}/(n_{Cl2(res)} + n_{O2}) = P_{O2}/(P_{Cl2(res)} + P_{O2}) \qquad (20\text{-}4)$$

where n^{o}_{Cl2} is the Cl_2 flow rate at the generator input, $n_{Cl2(res.),}$ and n_{O2} are flow rates of residual Cl_2 and O_2 in the generator. The $O_2(^1\Delta)$ partial pressure can be calculated from measured $O_2(^1\Delta)$ concentration, $c_{\Delta,}$ as $P_\Delta = c_\Delta R T$ (20-5)
and $O_2(^1\Delta)$ yield as $Y_\Delta = P_\Delta / P_{O2}$ (20-6)

Equation (20) follows then from eqs. (20-4) and (20-6).

Initial experiments (described in detail in the report [1]) were performed at the gas flow rates 60 mmol/s He, 2–35 mmol/s Cl_2, and BHP liquid flow rate of 8.5–10 ml/s. The generator pressure was in the range of 30–60 kPa (~225–450 Torr). The partial pressure of $O_2(^1\Delta)$ increased monotonically up to 4.5 kPa (34 Torr) with increasing chlorine flow rate. The calculated $U_{Cl}Y_\Delta$ product decreased from relatively high values 0.5–0.9 (at 2–6 mmol/s Cl_2) to 0.4 (at 17 mmol/s Cl_2), and then dropped to 0.2 (at 30–35 mmol/s Cl_2). Later experiments indicated that these results of $U_{Cl}Y_\Delta$ were somewhat overestimated due to an imperfect detection of $O_2(^1\Delta)$.

Following measurements were made with a new detection system working with 5 mm-Ge photodiode, a new interference filter, and professional amplifier (see chapter 3.3.2.). A great number of experiments were performed, when we tested the generator operation at different Cl_2 and He flow rates, BHP flow rate, generator pressure, and the separator rotation speed from 4000 r.p.m. to 9000 r.p.m. In experiments with 10–30 mmol/s Cl_2 and 60–80 mmol/s He, the product $U_{Cl}Y_\Delta$ attained only a medium value. One example of the dependence of $U_{Cl}Y_\Delta$ on the total generator pressure is shown in **Fig. 22,** and on the input Cl_2 pressure in the generator in **Fig. 23**. The experimental conditions are given in the figures captions. The measured decrease in $U_{Cl}Y_\Delta$ with increasing P_{gen} and chlorine pressure was certainly due to increasing $O_2(^1\Delta)$ loss in the quenching reactions (10)–(12).

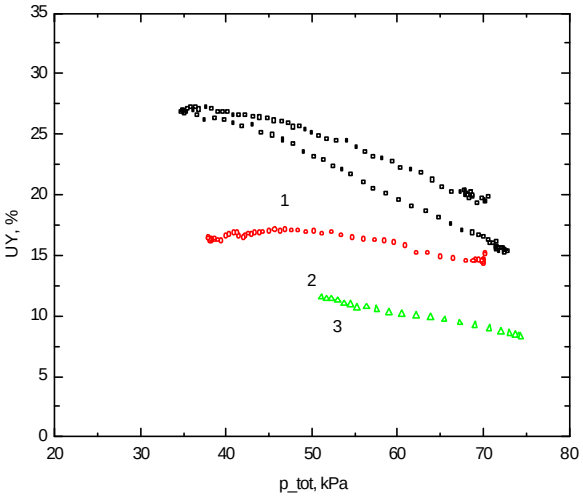

Fig. 22. $U_{Cl}Y_{\Delta}$ parameter in dependence on total generator pressure.

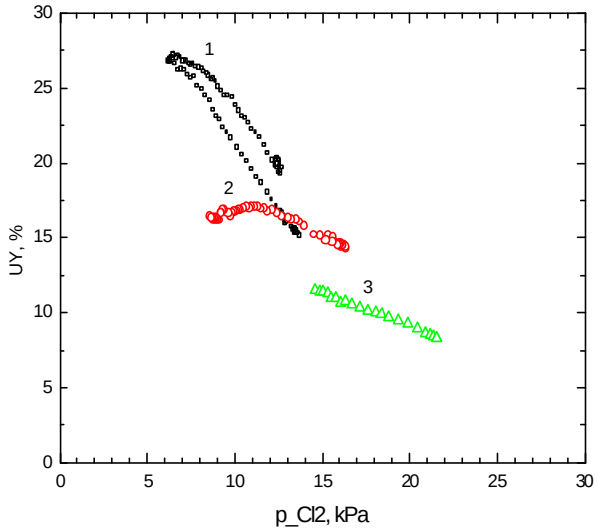

Fig. 23. Product $U_{Cl}Y_{\Delta}$ in dependence on chlorine input pressure in the generator.

Spray nozzle SAM-05-03; flow rates (in mmol/s): 13 Cl_2 + 60 He (curve 1), 17 Cl_2 + 60 He (curve 2), 24 Cl_2 + 60 He (curve 3); v_{BHP} = (8.1-9.5) ml/s; rotation speed 7000 r.p.m.

The obtained results proved that a limited production of $O_2(^1\Delta)$ in these experiments was most probably due to a long residence time of $O_2(^1\Delta)$ in the reaction space of the generator and the gas channels in separator rotor, and the stator body. A total reaction and transport time of gas in the system was calculated from the relation

$$\tau = V P_{tot} / (n R T) \qquad (21)$$

where V is the gas volume between the nozzle exit and the centre of the detection cell, P_{tot} is the total reactor pressure, n is the total molar gas flow rate, and T is the gas temperature. The dependence of $U_{Cl}Y_{\Delta}$ parameter on a calculated residence time (total reaction and transport time) for the experiment performed under conditions given in Figs. 22 and 23 is shown **Fig. 24**. The gas residence time was between 18 ms and 38 ms, which was significantly longer time than the optimum values (5–15 ms) for which the generator was initially designed (see chap. 2.2.). The residence time should be therefore shorter in order to reduce the $O_2(^1\Delta)$ losses. To achieve this, higher flow rates of helium were used in the next experiments. Example of the dependence of $U_{Cl}Y_{\Delta}$ product on the total generator pressure is shown in **Fig. 25.** A shorter gas residence time between 11 ms and 21 ms in this experiment resulted in higher $U_{Cl}Y_{\Delta}$ values in comparison with results in Fig. 22.

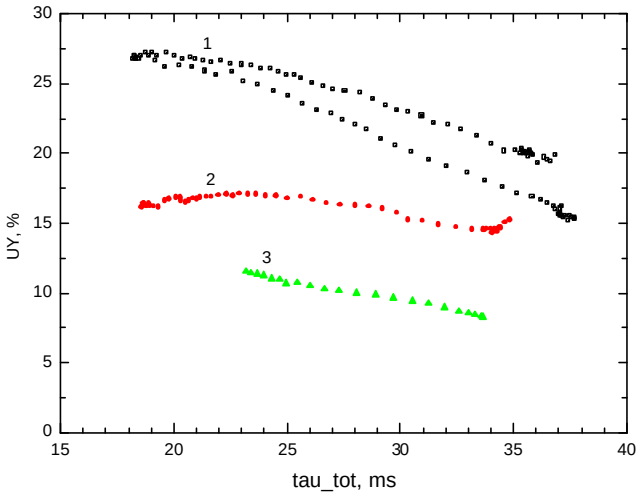

Fig. 24. $U_{Cl}Y_{\Delta}$ in dependence on gas residence time in the generator. The same conditions as in Figs. 25, 26

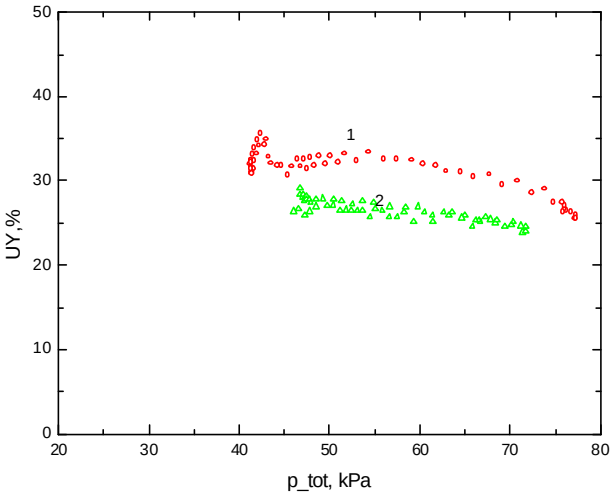

Fig. 25. $U_{Cl}Y_{\Delta}$ in dependence on the generator pressure Nozzle SAM-05-03, flow rates (in mmol/s): 15 Cl_2 + 120 He (curve 1), and 24 Cl_2 + 120 He (2); v_{BHP} = 10 ml/s; rotation speed 7000 r.p.m.

4.1.2. Measurements with separator rotor made of titanium

Similar measurements were performed with the separator rotor made of titanium because the heterogeneous $O_2(^1\Delta)$ loss should be, according to theoretical estimations significantly lower (see chap. 3.3.3.). Somewhat higher $U_{Cl}Y_{\Delta}$ values (by 10–20% relatively) were measured with Ti separator than with the stainless steel separator at 17 mmol/s Cl_2 and 120 mmol/s He. This result qualitatively agreed with data calculated for slit channels in the separator having one metallic wall (Ti) and one wall covered with a BHP film.

Significantly higher $U_{Cl}Y_{\Delta}$ values (up to nearly 60%) were measured when the He flow rate was still increased right to 160 mmol/s (see **Fig. 26**). This proved a positive effect of a shorter gas residence time in the generator, which was between 9 ms and 16 ms. The $U_{Cl}Y_{\Delta}$ product was very high for lower chlorine flow rates (7.5 and 10 mmol/s), however the chlorine pressure at the generator input was also low – see **Fig. 27**. A decrease in $U_{Cl}Y_{\Delta}$ with increasing chlorine flow rate could be caused by a higher $O_2(^1\Delta)$ loss and also too high BHP utilization at higher chlorine flow rates. By an assessment, the BHP utilization was 0.9 for the used BHP flow rate (with concentration of 5.4 M) at the highest Cl_2 flow rate of 26 mmol/s provided that U_{Cl} was 0.8. If we took into account existing droplet size distribution, the smaller BHP droplets were exhausted faster and could not further react with Cl_2 to produce $O_2(^1\Delta)$. This resulted in diminishing the chlorine utilization and thus the $U_{Cl}Y_{\Delta}$ product.

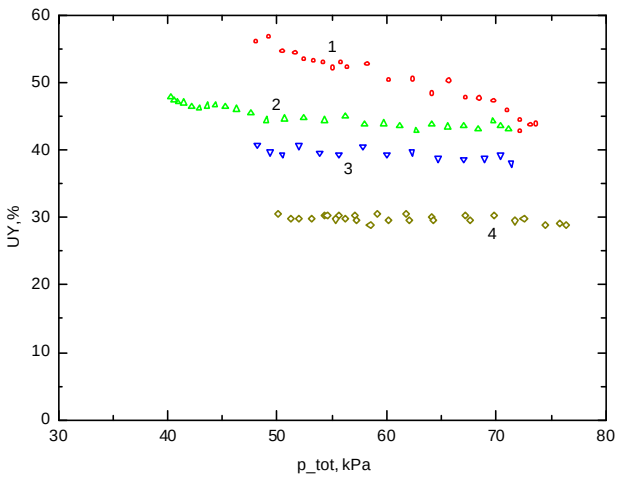

Fig. 26. $U_{Cl}Y_{\Delta}$ in dependence on total generator pressure.

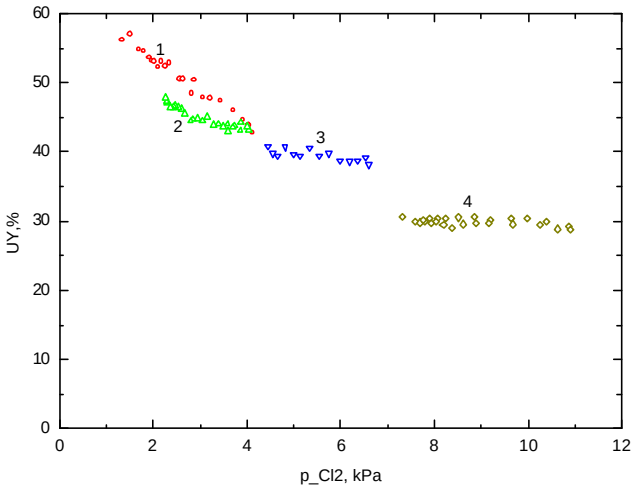

Fig. 27. $U_{Cl}Y_{\Delta}$in dependence on input chlorine pressure

Nozzle SAM-05-03; Ti rotor; gas flow rates (in mmol/s): 7.5 Cl_2 + 160 He (curve 1), 10 Cl_2 + 160 He (curve 2), 16 Cl_2 + 160 He (curve 3), 26 Cl_2 + 160 He (curve 4); v_{BHP} = 8.5 ml/s, 7000 r.p.m.;

To increase the BHP flow rate and gas flow rates, a larger spray nozzle SAM-06-04 in the CentSpraySOG device was employed in further study. The results of one experimental series are presented in **Figs. 28** and **29.**

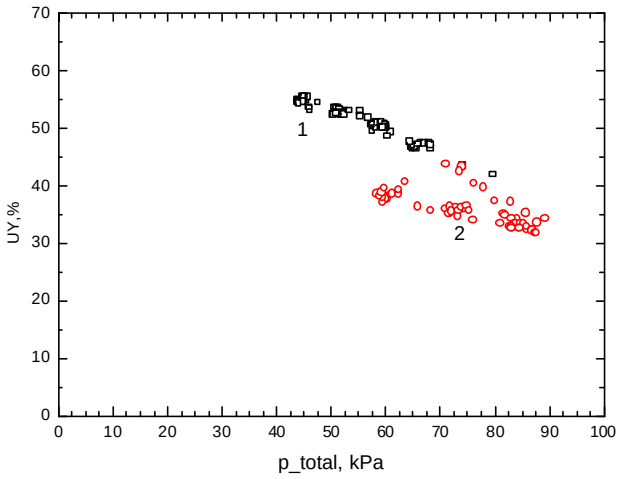

Fig. 28. $U_{Cl}Y_{\Delta}$ in dependence on total generator pressure.

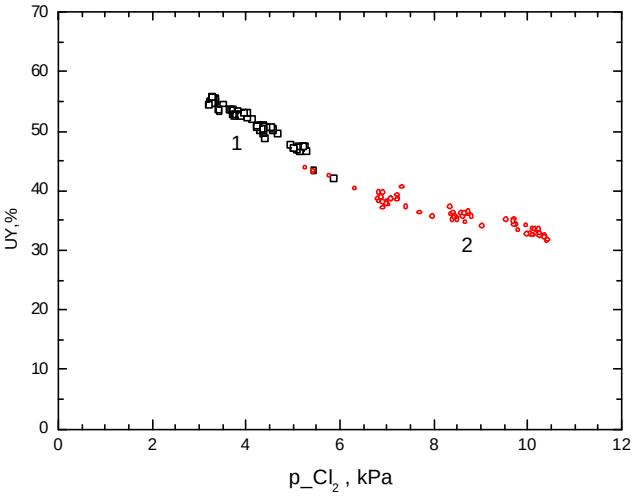

Fig. 29. $U_{Cl}Y_{\Delta}$ in dependence on input chlorine pressure.

Nozzle SAM-06-04; Ti rotor; gas flow rates (in mmol/s): 17 - 13 Cl_2 + 160 He (curve 1), 22 Cl_2 + 160 He (curve 2); v_{BHP} = 18 - 21 ml/s; 9000 r.p.m.

The $U_{Cl}Y_{\Delta}$ values obtained with the nozzle SAM-06-04 were higher by 6–10% as follows from comparing results in Fig 27 and 29. It can be explained by about twice higher BHP flow rate and corresponding lower BHP utilization. Partial pressure of $O_2(^1\Delta)$ was between 1.5 kPa and 3 kPa (10–20 Torr), and the $O_2(^1\Delta)$ yield decreased with increasing pressure from 65% to 45%.

The results of similar experiments measured with different helium flow rates are in **Figs. 30** and **31.** Partial pressure of $O_2(^1\Delta)$ was between 1.8 kPa and 3.5 kPa (13.5–26 Torr).

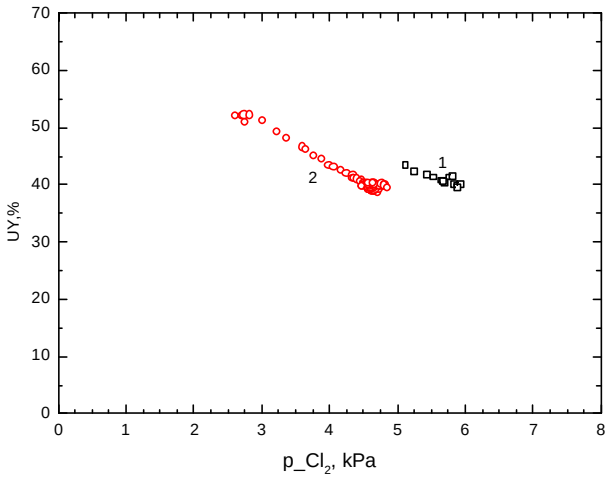

Fig. 30. $U_{Cl}Y_{\Delta}$ in dependence on input chlorine pressure.

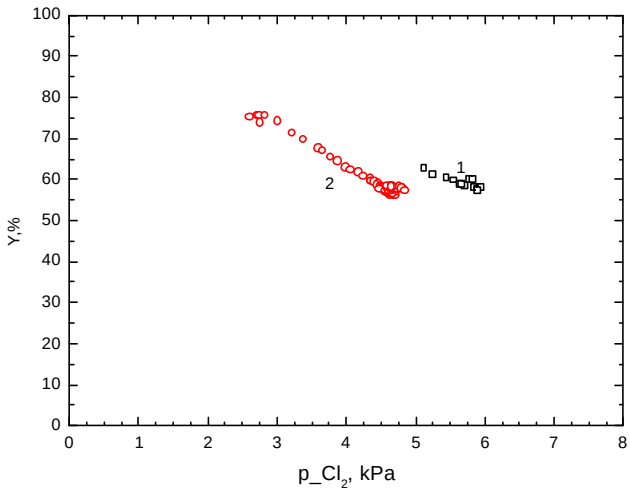

Fig. 31. Dependence of $O_2(^1\Delta)$ yield on input chlorine pressure.

Nozzle SAM-06-04; Ti rotor; gas flow rates (in mmol/s): 13 - 15 Cl_2 + 60 He (curve 1), 12 - 14 Cl_2 + 160 He (curve 2); P_{gen} = 30 kPa (curve 1), 50 - 60 kPa (curve 2); v_{BHP} = 21-22 ml/s; separator speed 9000 r.p.m.

In experiments with a lower He/Cl_2 ratio, the $U_{Cl}Y_{\Delta}$ product decreased to 0.42-0.22 at high input Cl_2 pressure, and the $O_2(^1\Delta)$ yield diminished with increasing P_{Cl2} from 68% to 31%. These results are given in **Figs. 32** and **33.** Partial pressure of $O_2(^1\Delta)$ was between 2.2 kPa and 3.6 kPa (16.5–27 Torr), and U_{Cl} was 0.64–0.68.

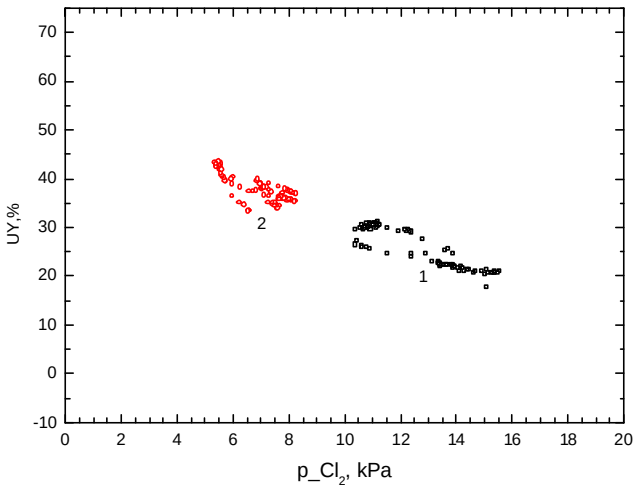

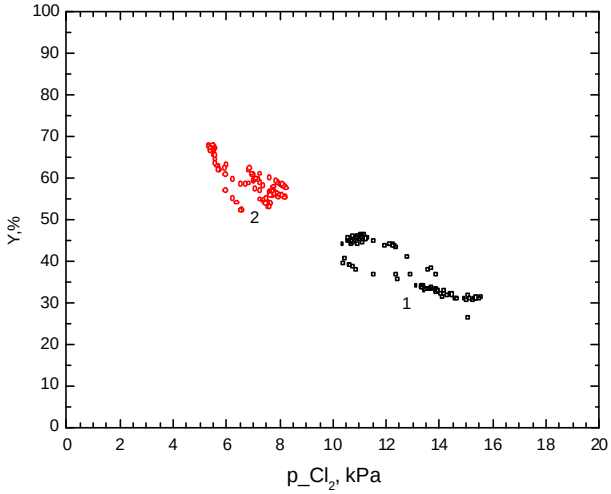

Fig. 32. $U_{Cl}Y_{\Delta}$ in dependence on input chlorine pressure. **Fig. 33**. Dependence of $O_2(^1\Delta)$ yield on input chlorine pressure.

Nozzle SAM-06-04, Ti rotor; gas flow rates (in mmol/s): 20 Cl_2 + 90 He (curve 1), 16.5 Cl_2 + 160 He (curve 2); P_{gen} = 60 - 85 kPa; v_{BHP} = 14.5 – 16.5 ml/s; 9000 r.p.m.

The results given above has been chosen as the representative examples of tens experiments on the CentSpraySOG device performed by termination of the Contract. More results inclusive the auxiliary experiments, supporting calculation and modeling were presented in previous Reports [14–20], and some were gathered only recently.

Finally, we compared the $U_{Cl}Y_{\Delta}$ values determined with our centrifugal spray generator with some data given in literature for the rotating disc and jet generators operating also with the Cl_2/He mixture (see **Table 6**). Our values obtained for a lower input chlorine pressure that are also typical for generators with rotating discs or jet generators (1.6 to 4 kPa) were close to data in the papers [22] – [24] but lower than in the papers [26] and [27]. The total generator pressure was however substantially higher in our system. The data on $U_{Cl}Y_{\Delta}$ measured in CentSpraySOG decreased with increasing input chlorine pressure to 33%, and further to 20% at highest chlorine pressures, but the comparison with other generator types was impossible because they could not operate with such high chlorine pressure (except for a jet generator operating with Cl_2 only (without a buffer gas); the total generator pressure was however several times lower.

Tab. 6
Survey of SOG main parameters

Authors	n_{Cl2} mmol/s	n_{He} mmol/s	P_{gen} Torr	P_{gen} kPa	P_{Cl2} kPa	U_{Cl} %	Y_D %	$U_{Cl}Y_D$ %
Kendrick *et al.* [22]	532	1500	44	5.9	1.5	95	52	49
Rittenhouse *et al.* [23]	71	280	60	8	1.6	94	54	50
McDermott *et al.* [24]	250	750	100	13.3	3.3	88	55	48
Nikolaev *et al.* [25]	33	90	36	4.8	1.3	93	-	-
Blayas *et al.* [26]	10	20	91	12	4	95	80	76
Watanabe *et al.* [27]	38	497 N_2	5-40	0.6-5.3	<0.4	99	55-90	54-89
This Report	7.5-10	160	340-550	45-73	1.6-4	-	-	45-56
This Report	13-22	160	340-650	45-87	3-10	-	-	33-55
This Report	20	90	450-640	60-85	10-15	64-68	30-45	30-20

5. Summary

Department of Chemical Lasers at the Institute of Physics, Academy of Sciences CR in Prague proposed and investigated theoretically and experimentally an advanced concept of the singlet oxygen generator (SOG), a centrifugal spray generator (CentSpraySOG), for driving a chemical oxygen-iodine laser (COIL). This generator operates with a conventional gas-liquid chemical reaction of chlorine and basic hydrogen peroxide (BHP) similarly as e.g. a jet or rotating disk generator employed hitherto in the COIL technology. The novel CentSpraySOG takes advantage of a droplet spray system with a large interface area for the reaction, and separation of exhausted BHP liquid from generated singlet oxygen, $O_2(^1\Delta)$ by the centrifugal force. A high $O_2(^1\Delta)$ partial pressure at high total generator pressures could be expected in optimal SOG operation, independent on the device frame acceleration and gravitation. This would be beneficial for a mobile COIL unit.

The computational modeling provided essential data for the generator design and operation parameters, e.g. a spray droplet size for efficient high pressure $O_2(^1\Delta)$ generation, and configuration and dimensions of the centrifuge for efficient gas-liquid separation. Modeling of the spray SOG was performed for a specific commercial spray nozzle (SAM-05-03) producing a homogeneous BHP spray with droplets of ~20 μm in diameter, and for realistic flow rates of BHP and gases (15 ml/s BHP (8M or 5 M), and 23 mmol/s Cl_2 + 92 mmol/s He). The results showed that this generator could generate high yields of singlet oxygen (up to 0.8) with a high chlorine utilization (0.75–0.95) and BHP utilization (36–54%).

The nozzles SAM-type with external mixing of gas-liquid media were chosen after a comprehensive survey of available commercial nozzles, suitable for atomization of a viscous BHP liquid in the SOG conditions. Supporting measurements of the droplet size in a spray of BHP-like model liquid (70% glycerol in water) by the special instrument based on laser beam diffraction helped to find the input gas and liquid pressure to generate the BHP spray of sufficiently small droplets (a mean diameter ≤ 20 μm). A BHP spray temperature estimated from a heat balance of the reaction system was relatively high (30–50°C). It resulted in relatively high water vapor pressure in $O_2(^1\Delta)$ exiting the generator. A detrimental effect of water on lasing could be however diminished by a supersonic injection of atomic iodine into the COIL cavity.

The results of detailed parametric investigations performed on the stationary spray SOG (without a separator) proved that the $O_2(^1\Delta)$ partial pressure increased up to 4 kPa (30 Torr) at the generator pressure of 60–70 kPa (450–525 Torr). A rather high $U_{Cl}Y_{\Delta}$ (product of Cl_2 utilization and $O_2(^1\Delta)$ yield used for the SOG evaluation) in the range of 0.6–0.8 was attained at the generator pressure of 20–30 kPa (150–225 Torr), or 0.4–0.6 at 40–60 kPa (300– 450 Torr), respectively. This was in a good agreement with results of modeling.

A two-step gas-liquid separation in the CentSpraySOG was suggested: *i)* separation of larger droplets by impact (by estimation 99% of droplets ≥3.2 μm should be separated), and *ii)* separation of remaining finer droplets by the centrifugal force in narrow slit channels (this should remove droplets ≥ 0.5 μm at the rotation speed of 5000 r.p.m. The analysis showed that a major loss of singlet oxygen in the proposed separator is due to the gas phase pooling and quenching reactions. The 82% $O_2(^1\Delta)$ yield at reaction space outlet would be reduced to 69% at the stator outlet. A design of the separator parameters and its manufacturing issued from these modelling results.

A fabricated CentSpraySOG device assembled with gas and liquid management, diagnostic techniques and PC data acquisition system was experimentally investigated. Separation tests were performed first with introducing water or model liquids (70% aqueous solution of glycerol or 32% NaOH solution) and gas (helium or nitrogen). Tests with 32% NaOH (flow rate up to 7.2 ml/s) and nitrogen (up to 50 mmol/s) at atmospheric pressure proved that nearly no aerosol was visible in the exiting gas (at 4000 r.p.m.). Similar tests were performed at pressure range of 25 kPa (~188 Torr) to 100 kPa (750 Torr). No droplets were observed in the gas exiting the separator at the rotation speed 4000 r.p.m. with the model liquid (32% NaOH, 10 ml/s), and 60 mmol/s He + 36 mmol/s N_2. During these tests, several constructional modifications of the device had to be fabricated.

The gas-liquid separation with the reactive BHP/Cl_2 system at sub-atmospheric pressures was more difficult. It was improved by adjusting a pressure difference between the gas exit and the BHP exit from the device, and by increasing the rotation speed. The exiting gas was visually free of droplets at 6000 r.p.m., flow rates of 90 mmol/s He + 25 mmol/s Cl_2, and generator pressure ≥ 50 kPa (375 Torr). A rough estimate of entrained alkali during one operation was made by the acidimetric titration of a felt inserted in the optical cell located just at the generator exit. The separation efficiency determined from this test was very high (99.96%), and the aerosol concentration in the optical cell was 0.36 ppm only.

Modeling of homogeneous and heterogeneous $O_2(^1?)$ losses in all spaces of the separator and on the walls was made. These results showed that the heterogeneous $O_2(^1?)$ loss in the narrow slit channels in the rotor can be significant due to a short diffusion path and high $O_2(^1?)$ accommodation (deactivation) coefficient on the stainless steel used for the rotor fabrication. Titanium was therefore chosen for fabrication of another rotor of CentSpraySOG separator because of much lower (by two orders) $O_2(^1?)$ accommodation coefficient and good corrosion resistance.

First experiments with Cl_2/BHP reaction system in CentSpraySOG has shown that the $O_2(^1?)$ partial pressure increased up to 4 kPa (30 Torr) with increasing chlorine flow rate (and at generator pressure 30–60 kPa (~225–450 Torr). The product $U_{Cl}Y_\Delta$ decreased with increasing total generator pressure and also with the chlorine pressure at the generator input. The $U_{Cl}Y_\Delta$ values were also very dependent on the gas residence time in the generator, which has a substantial effect on $O_2(^1?)$ loss. Lowest $U_{Cl}Y_\Delta$ values (0.08–0.28) were obtained for the lowest He flow rate (60 mmol/s He), when the gas residence time was too long (18–38 ms). Medium $U_{Cl}Y_\Delta$ (0.24–0.35) was obtained for medium He flow rate (120 mmol/s), when the gas residence time was 11–21 ms. The highest $U_{Cl}Y_\Delta$ (0.3–0.57) was measured with 160 mml/s He reducing the gas residence time to 9–16 ms.

Experiments on the CentSpraySOG with titanium separator rotor provided fairly higher $O_2(^1\Delta)$ generation efficiency. The values of $U_{Cl}Y_\Delta$ parameter were in the range of 0.30–0.6 at the flow rates 160 mmol/s He and 7.5–26 mmol/s Cl_2. The total generator pressure varied between 40–75 kPa (300–560 Torr). Much effort was recently devoted to measurements of residual chlorine concentration by spectrometric detection to be able to evaluate separately the chlorine utilization, U_{Cl}, and singlet oxygen yield, Y_Δ. A typical value of U_{Cl} was between 0.64 and 0.84, i.e. slightly lower than values obtained by modeling (0.74-0.88) for the used 5M BHP. This difference can be ascribed to a non-uniform droplet size distribution resulting in a faster BHP exhausting in smaller droplets that limited $O_2(^1\Delta)$ production. The measured $O_2(^1\Delta)$ yield varied between 0.30 and 0.75. The difference between initially calculated values was due to $O_2(^1\Delta)$ loss in the separator gas channels, and also in the optical cell.

By the termination of the Contract, typical parameters of CentSpraySOG were Y_Δ <0.75 – 0.3>, U_{Cl} <0.64 – 0.84>, and $O_2(^1\Delta)$ partial pressure <2.2 – 4 kPa> (16.5–27 Torr), measured at the generator pressure of 45–85 kPa (~340–640 Torr). Conditions of rather effective liquid separation from the exiting gas were estimated. The separation of BHP droplets was however not always quite reproducible.

Comparing our data with similar parameters published on rotating disc and jet generators has shown that the CentSpraySOG could operate at much higher generator pressure, and also with a higher chlorine pressure at the generator input.

6. Conclusion

The tasks and supplies in the Contract proposal for the research periods I – III of this Contract that are given in pages 3 and 4 of this report were all fulfilled, except for the last task: Testing the CentSpraySOG device coupled to a 5-cm-gain COIL nozzle plenum. Despite our great effort, some constructional modifications of the device could not be speed up, and solving some technical problems with the gas-liquid separation also took more time than we expected.

References

[1] P. V. Danckwerts, *Gas-liquid reactions,* McGraw-Hill, NY, 1970

[2] B. R. Bird, W. E. Stewart, and E. N. Lightfoot, *Transport Phenomena,* p. 42, John Wiley, 2nd ed., NY, 2002

[3] N. G. Basov, M. V. Zagidullin, V. I. Igoshin, V. A. Katulin, and N. L. Kuprianov, "Theoretical analysis of chemical oxygen-iodine lasers," *Trudy FIAN RAS (in Russian)* **171**, pp. 30-53,1986

[4] J. A. Blauer, S. A. Munjee, K. A. Truesdell, E. C. Curtis, and J. F. Sullivan, "Aerosol generators for singlet oxygen production," *J. of Appl. Phys*. **62**, pp. 2508-2517, 1987

[5] M. V. Zagidullin, V. I. Igoshin, V. A. Katulin, and N. L. Kuprianov "A possible utilization of spray medium for chemical generator of singlet oxygen for oxygen-iodine laser," *Quantum Electronics (in Russian)* **10**, pp. 797-801, 1983

[6] W. C. Hinds, *Aerosol Technology*, New York, Wiley, 1999

[7] J. Kodymová, J. Hrubý, O. Špalek, V. Jirásek, M. Censký, M. V. Zagidullin, V.D. Nikolaev, M.I. Svistun, and N.I. Khvatov, „Advanced concepts of singlet oxygen generator for a chemical oxygen-iodine laser, 36th AIAA Plasmadynamics and laser Conference , Toronto, ON, Canada, 2005, AIAA Paper 2005-**5166**

[8] O. Špalek, J. Hrubý, V. Jirásek, M. Censký, J. Kodymová, and I. Picková, "Advanced spray generator of singlet oxygen", Proc. SPIE Vol. **6346**, 6346OC1-OC9, 2006

[9] J. Kodymová, O. Špalek, V. Jirásek, M. Censký, and I. Picková, "A centrifugal spray singlet oxygen generator for a chemical oxygen-iodine laser", 38th AIAA Plasmadynamics and Lasers Conference, Miami, FL, USA, 25-28 June 2007, AIAA Paper **2007-4622,** CD Proceedings

[10] Interim Report 001 – Research Phase 1 of this Contract #FA8655-05-C-4022, submitted 31 May 2005

[11] Interim Report 002 – Research Phase 1 of this Contract #FA8655-05-C-4022, submitted 30 August 2005

[12] Interim Report 003 – Research Phase 1 of this Contract #FA8655-05-C-4022, submitted 30 November 2005

[13] Final Report of Research Phase 1 of this Contract #FA8655-05-C-4022, submitted 28 February 2006

[14] Interim Report 001 – Research Phase 2 of this Contract #FA8655-05-C-4022, submitted 1 June 2006

[15] Interim Report 002 – Research Phase 2 of this Contract #FA8655-05-C-4022, submitted 1 September 2006

[16] Interim Report 003 – Research Phase 2 of this Contract #FA8655-05-C-4022, submitted 1 December 2006
[17] Final Report of Research Phase 2 of this Contract #FA8655-05-C-4022, submitted 28 February 2007
[18] Interim Report 001 – Research Phase 3 of this Contract #FA8655-05-C-4022, submitted 28 July 2007
[19] Interim Report 002 – Research Phase 3 of this Contract #FA8655-05-C-4022, submitted 31 October 2007
[20] Interim Report 003 – Research Phase 3 of this Contract #FA8655-05-C-4022, submitted 31 January 2008
[21] P. D. Whitefield, D. E. Hagen, M. B. Trueblood, and W. M. Barnett, "Experimental investigation of homogeneous and heterogeneous nucleation condensation processes and products in COIL", SPIE Proc., Vol. **1871**, 277 (1993)
[22] K. R. Kendrick, Ch. A. Helms, and B. G. Quillen, "Determination of singlet oxygen generator efficiency in a 10/kW class supersonic chemical oxygen-iodine laser (RADICL)", IEEE J. Quant. Electron. **35**, 1759 (1999)
[23] T. L. Rittenhouse, S. P. Phipps, and Ch. A. Helms, "Performance of a high-efficiency 5-cm gain length supersonic chemical oxygen-iodine laser", IEEE J. Quant. Electron. **35**, 857 (1999)
[24] W. E. McDermott, J. C. Stephens, J. Vetrovec, and R. A. Dickerson, "Operating Experience with a high throughput jet generator" 28th Plasmadynamics and Lasers Conference, Atlanta, GA, AIAA Paper **97-2385**
[25] V. D. Nikolaev, M. I. Svistun, M. V. Zagidullin, and G. D. Hager, „Efficient chemical oxygen-iodine laser powered by a centrifugal bubble singlet oxygen generator" , Appl. Phys. Lett. **86**, 1 (2005)
[26] I. Blayas, B. D. Barmashenko, D. Furman, S. Rosenwakd, and M. V. Zagidullin, "Power optimization of small-scale chemical oxygen-iodine laser with jet-type singlet oxygen generator", IEEE J. Quant. Electron. **32,** 2051 (1996)
[27] G. Watanabe, D. Sugimoto, K. Tei, and T. Fujioka, "Optimization of jet-type singlet oxygen generator for ejector –COIL", Proc. SPIE Vol. **5777**, 49, 2004

Acknowledgements

The investigators are very grateful to the US AFRL/DED at Kirtland AFB, NM for the financial support of this research via the USAF EOARD Contract.

We wish to thank Dr. Timothy Madden and Dr. Kevin Hewett at the US AFRL/DED for beneficial discussions on the contract tasks and encouragement.

We thank Dr. A. Gavrielides, Program Manager Lasers and Electro-Optics, Mrs. Susan Fuller, Contracting Officer, and Mrs. Jeannette Cyrus, Program Analyst at the USAF EAORD for their very valuable assistance with the Contract processing.